1992ApJ...391...16S

THE ASTROPHYSICAL JOURNAL, 391:16–33, 1992 May 20
© 1992. The American Astronomical Society. All rights reserved. Printed in U.S.A.

NEARBY GALAXY FLOWS MODELED BY THE LIGHT DISTRIBUTION

EDWARD J. SHAYA
Columbia University[1]
R. BRENT TULLY[2]
University of Hawaii
AND
MICHAEL J. PIERCE
Dominion Astrophysical Observatory[3]
Received 1990 November 28; accepted 1991 November 13

ABSTRACT

The observed distribution of light in the Local Supercluster has been used to determine the expected velocities of galaxies if the assumptions are valid that nonexpansion motions are generated by gravitational perturbations and that mass is distributed like the light. Since detailed knowledge of the light distribution extends to only 3000 km s^{-1}, three extra sources are added at large distances: one associated with the Great Attractor, one loosely with the Perseus-Pisces Supercluster region, and one with the Shapley Concentration at a distance corresponding to 13,800 km s^{-1}. The nearer two sources are motivated by improvements they offer to χ^2 fits while the distant source is required to get agreement with the cosmic microwave background dipole. Comparison is made with observed velocity field maps based on 301 high-quality distance estimates in 142 groups and 53 individual galaxies.

The assumption that gravitational perturbations must dominate the generation of peculiar velocities is substantiated and $M/L \simeq 144h\Omega_0^{0.4}$ is found. A surprisingly strong conclusion can be drawn that the clumped mass is clustered on scales of less than 1 Mpc with $M/L \sim 100$ and that an *insignificant* amount of additional mass is clustered on scales between 1 Mpc and ~20 Mpc. A value of $\Omega_{gal} \sim 0.03$–0.1 is associated with clumped mass. The location of the three sources beyond 3000 km s^{-1} involves some speculation, but a curious influence of these long-range forces is a slowing of the merger of the nearest groups. There are hints of velocity streaming with coherence over 20,000 km s^{-1} and mass fluctuations on 10^{17} $M_\odot$ scales. The model provides a natural description of the "local velocity anomaly." The χ^2 fit for the preferred model results in an equivalent rms uncertainty in the difference between observed and model velocities of 18% of the observed velocity.

Subject headings: cosmology: observations — galaxies: clustering — galaxies: distance and redshifts

1. BACKGROUND

Over the last decade, there has been the development of an increasingly complex view of the motions of nearby galaxies. Once it was possible to argue that departures from Hubble expansion are extremely small (Sandage 1972). There were early hints, though, that there are substantial "non-Hubble" motions on a variety of scales (Rubin 1951; de Vaucouleurs 1958; de Vaucouleurs & Peters 1968; Rubin et al. 1976). As it became convincing that the Local Supercluster has a strong perturbing affect on our motion, simple models were developed based on spherically symmetric distributions of mass centered on the Virgo Cluster (Tony & Davis 1981; Hoffman, Olson, & Salpeter 1980; Hoffman & Salpeter 1982; Aaronson et al. 1982a; Tully & Shaya 1984).

During this period, the recently discovered anisotropy in the cosmic microwave background came to be interpreted as evidence for a motion with respect to the surface of last scattering. The current value of the velocity of the Sun is 360 km s^{-1} toward $l = 265$ $b = 50$ (Lubin & Villela 1986). It was pointed out by Shaya (1984) and Tammann & Sandage (1985) that a Virgocentric model could not fully account for this motion and that there must be residual flow in the direction of the Hydra-Centaurus region, identified to contain a nearby supercluster by Chincarini & Rood (1979).

This proposition gained a much sounder footing with the discovery of a large-scale flow with three-parameter Faber-Jackson distances to elliptical galaxies (Dressler et al. 1987). The preferred model quickly evolved to that of the "Great Attractor," an excess of mass of perhaps 5×10^{16} $M_\odot$ at 4200 km s^{-1} distance in the Centaurus constellation (Lynden-Bell et al. 1988; Dressler 1988; Aaronson et al. 1989; Staveley-Smith & Davies 1989; Burstein, Faber, & Dressler 1990). To date, the most elaborate parametric model that has been developed to describe the observed non-Hubble motions is by Faber & Burstein (1988) and includes three components: an extended Great Attractor, an extended Virgo Cluster, and a "local anomaly" (also Han & Mould 1990). The Great Attractor model has two particularly attractive features. The first is that it is in the right direction and, plausibly, could have the right amplitude to explain the cosmic microwave background anisotropy. The second is that mass at the Great Attractor location would provide tidal distention along the connecting

[1] Physics Department, University of Maryland, College Park, MD 20742.
[2] On leave at the Istituto di Radioastronomia, CNR, Bologna, Italy, during the period of this research. Postal address: Institute of Astronomy, University of Hawaii, 2680 Woodlawn Drive, Honolulu, HI 96822.
[3] National Optical Astronomical Observatories, P.O. Box 26732, Tucson, AZ 85726-6732.

© American Astronomical Society • Provided by the NASA Astrophysics Data System

1992ApJ...391...16S

axis and compression in orthogonal directions, in agreement with observations as first noted by Lilje, Yahil, & Jones (1986).

A recent development has been the new view of our neighborhood afforded by the *IRAS* survey (Meiksen & Davis 1986; Yahil, Walker, & Rowan-Robinson 1986) especially now that redshifts are available (Strauss & Davis 1988; Yahil 1988). Particularly, the beautiful work by Yahil has shown that there is general agreement between flow patterns that are *anticipated* if mass is distributed like the *IRAS* galaxies and the non-Hubble motions that are *seen* in the samples of elliptical and spiral galaxies with distance estimates compiled by Faber & Burstein (1988). Yahil was already willing to conclude that large-scale structure must be basically gravitational in origin.

Yahil confirmed that we participate in a flow toward the Great Attractor direction but it is worth noting that he found the peculiar velocity on the Sun to be generated within 4000 km s^{-1}, a value smaller than might be expected from an extended Great Attractor. A similar picture emerged from the work by Lynden-Bell & Lahav (1988), who find that the largest part of the acceleration due to the observed distribution of visible galaxies is associated with galaxies nearer than half the Great Attractor distance.

An interesting approach to the problem is currently being developed by Bertschinger & Dekel (1989; Dekel & Bertschinger 1990; Bertschinger et al. 1990). Their procedure is to use observed peculiar velocities to derive a three-dimensional map of the potential field and, hence, of the smoothed distribution of mass. These maps can be compared with maps of the distribution of galaxies to see if there is any resemblance. Using basically the same information on peculiar velocities as available to Faber & Burstein (1988), these authors are recovering the main features of the light-distribution maps. Minor exceptions will be mentioned in a later section.

We come to what we hope to contribute to this discussion. We can go farther because of two elements of observational material. The first is a particularly detailed map of the distribution of light in the volume within 3000 km s^{-1}, based on the Nearby Galaxies Atlas (Tully & Fisher 1987; hereafter NBG atlas). It is true that the *IRAS* maps (Yahil 1988) provide information to a depth of $\sim$10,000 km s^{-1} and are less hampered by losses at low galactic latitude. However, our maps based on visible light contain more information within our limited volume and more fairly sample the high-density regions dominated by systems with old stellar populations. The region of particular interest to us in this study lies within 2000 km s^{-1}. Structure on the larger scales mapped by the *IRAS* sample may well affect our local region, so we make crude use of the information that the *IRAS* sample affords.

Our second observational element is a newly extended sample of spiral galaxies with accurately measured distances, which can be used to map non-Hubble flows. Our distances are derived from the luminosity–H I profile line width method (Tully & Fisher 1977; hereafter TF method), using both aperture H-band (Aaronson, Huchra, & Mould 1979) and CCD-measured (Pierce & Tully 1988) *B,R,I*-band luminosities. The *H*-band material is from Aaronson et al. (1982b) and has been used for similar purposes by Aaronson et al. (1982a) and Faber & Burstein (1988). To this data base, we have added CCD material on 68 field galaxies, 41 in common to the H-band sample and 27 new. There is also the extensive CCD material discussed by Pierce & Tully on the Virgo and Ursa Major clusters that anchor our maps of distances. In the next section, we will discuss some areas of improvements in the presently compiled distance estimates. With respect to Faber & Burstein (1988), there are differences in how we deal with Malmquist bias.

In the linear approximation, there is a direct relationship (Peebles 1980) between the distribution of mass, which we infer from the light, and the peculiar velocities of test particles. We measure the radial component of peculiar velocity by taking the difference between the observed velocity of a galaxy and $H_0 d$, where d is our measured distance and H_0 is the Hubble Constant. For the purpose of mapping deviant velocities, the zero-point in the evaluation of H_0 does not matter.

The zeroth-order question that we ask in this paper is whether the observed distribution of galaxies produces a model of the velocity field that bears a resemblance to the observed velocity field in the local vicinity. In the simplest case, we have two free parameters: the mass-to-light ratio we assign to the observed galaxies within 3000 km s^{-1} and the value of Ω_0 we associate with the mean density of matter beyond 3000 km s^{-1}. The details of the model will be described in a later section. In our preferred model, we also include gravitational contributions from Great Attractor, Perseus-Pisces, and Shapley mass concentrations beyond 3000 km s^{-1}.

2. THE SAMPLE OF GALAXIES WITH DISTANCES

Distances are determined by The TF method, making use of both literature near-infrared H-band luminosities (Aaronson et al. 1982b) and *B,R,I*-band luminosities recently obtained with wide-field CCD cameras at Mauna Kea Observatory (Pierce 1992). Neutral hydrogen line widths are drawn from the Nearby Galaxies Catalog (Tully 1988a; hereafter NBG catalog), adjusted to be statistically equivalent to twice the maximum rotation velocity (Tully & Fouqué 1985).

The relative merits of the various photometric passbands are discussed by Pierce & Tully (1988). Luminosities are corrected for reddening in all passbands, including H, in the manner described by Tully & Fouqué (1985) and Pierce & Tully (1988). A special virtue of the CCD material comes from the ability to derive inclinations with photometric accuracy, and we argue that the rms uncertainty in inclinations is improved from $\pm 7°$ to $\pm 3°$. In cases where these inclinations can be used with H-band material, we find the scatter in *R*, *I*, and *H* bands to be comparable, in the range 0.3–0.4 mag or corresponding to 15%–20% in distance.

A particularly important point to mention is our procedure to bypass Malmquist bias. The issue is discussed elsewhere (Tully 1988b, 1989a), but here is a brief summary. The problem to be avoided is the tendency to select galaxies that are brighter than a mean relation in magnitude-limited samples, a tendency that can cause a progressive underestimation of distances to systems that are further away. This problem can be circumvented in our case if we have access to a volume-limited sample of comparable observational quality and if we take our mean relation to be the regression on the distance-independent variable, the H I profile line width. This procedure requires two assumptions: that the H I line widths are measured without bias and that the galaxies in the volume-limited reference sample have similar properties to those in the sample to be considered subsequently. With the regression on line width, then at a given magnitude there is an equal probability of drawing a galaxy with a positive or negative line width offset from the mean relation. Hence, the distance estimate is as likely to be too large as too small.

© American Astronomical Society • Provided by the NASA Astrophysics Data System

1992ApJ...391...16S

The condition that line-widths be unbiased is close to true in the present study of nearby systems because sufficient signal to noise usually can be obtained in the H I line with modest integrations. The volume-limited sample that provides the TF regression is the Ursa Major Cluster where we have reasonable completeness to $B_T^{b,i} = 13.3$, or $M_b^{b,i} = -17.7$ (Pierce & Tully 1988). The conditions in this low-density cluster and the morphological characteristics of the overwhelmingly late-type galaxies give us reason to expect that the sample is representative of galaxies in many other environments in the Local Supercluster (possible problems in B band: see Pierce & Tully 1991). If the two previously mentioned assumptions are correct, then Monte Carlo simulations that were discussed in the previously cited references have confirmed that our distance estimates will be free of bias.

It is to be appreciated that a data set free of systematic distance estimate biases may still contain some biases in a map of peculiar velocities. For example, in the case of a uniformly sampled homogeneous universe, the volume effect means that in a given shell about us there will be more galaxies erroneously thrown foward from the background than thrown background from the foreground. Hence, there would be more mistaken positive peculiar velocities than negative in the shell. The more complicated bias corrections by Lynden-Bell et al. (1988) account for this density-distribution effect *in the specific case of a homogeneous universe.*

Since the universe is evidently *not* homogeneous on the relevant scales, it is not obvious that one is better off making this particular assumption. More sophisticated iterative procedures can be entertained to correct the peculiar velocity map for density fluctuations but we have not made any such attempt. It is our expectation that the density-distribution bias will be a minor effect in our sample.

Our measured distances are recorded in Table 1 of the companion Astrophysical Journal article Supplement by Tully, Shaya, & Pierce (1992, hereafter TSP). If galaxies are assigned to groups (Tully 1987, 1988a) then the distance estimate is the average of the individual TF distances for group members. The group is assigned a velocity which is the average over *all* group members. The averaging of distance estimates and velocities substantially reduces measurement uncertainties.

In all, TSP provides information regarding 600 distance measurements of 301 galaxies. These include 26 galaxies in each of the Virgo and Ursa Major clusters, 196 galaxies in 140 smaller groups, and 53 individual galaxies. Although the zero point is unimportant, we note that the Virgo Cluster is placed at 15.6 Mpc, consistent with $H_0 = 88$ km s^{-1} Mpc^{-1} with a cluster velocity of 1370 km s^{-1}. The CCD sample presented here is only a small fraction of what we will soon have available. The current material is from Pierce (1991) and is drawn from a sample of spirals nearer than Virgo, with $\delta > -40°$, and $M_B^{b,i} < -18.4 + 5 \log h$, where $h = H_0/100$. We are reducing three-band CCD material on an extended sample of $\sim$700 galaxies, so we will eventually be able to do an analysis with much more data.

3. MODEL OF THE MASS DISTRIBUTION

The basis for our model of the mass distribution is the observed distribution of light associated with galaxies in the NBG atlas and catalog (Tully & Fisher 1987; Tully 1988a). The important properties of this sample are described by Tully (1988c). One point to note is the assertion that the NBG atlas is reasonably homogeneous across the sky except for the effects of obscuration because it is dominated by two all-sky samples: for early-types, by the magnitude-limited revised Shapley-Ames sample (Sandage & Tammann 1981) and, for late types, by a sample observed in the H I line after a search for candidates over the entire northern and southern sky atlases by one of the authors (R. B. T.). The other key point is that the incompleteness with distance in the NBG atlas is relatively well understood. In Tully (1988c), a correction, F_L, is derived for the light associated with galaxies missing from the catalog because of incompletion, which can be rewritten in a form independent of the distance scale:

$$F_L = \exp\{4.21[\log(V_0/750)]^{2.82}\} . \quad (1)$$

where V_0 is the systemic velocity of a galaxy. In this form, this correction factor is only statistically correct since it has been applied in the framework of the NBG catalog where distances are assigned based on a Virgocentric kinematic model. The correction factor flairs up rapidly, from unity below $V_0 = 750$ km s^{-1} to $F_L \simeq 3$ at $V_0 = 3000$ km s^{-1}, the catalog limit.

It is evident that the NBG atlas only provides information of statistical relevance beyond $V_0 \simeq 1500$ km s^{-1}. Also, this source provides no information beyond $V_0 = 3000$ km s^{-1}. Since our information is still so incomplete, it seemed justified to generate a "reduced" three-dimensional map of the light distribution. We again draw upon the group catalog (Tully 1987) and sum over all the absorption-corrected light of group members, correct by the light incompletion factor that depends upon distance, and make one entry in the "reduced" map at the barycenter of the group. Galaxies identified as standing alone or only loosely "associated" with groups in the NBG catalog are treated individually, but receive the same statistical correction to their light to account for the galaxies at their same distance that are missed. Presumably, a lot of the missing objects are distributed somewhat like the observed systems.

In this way, we generate a map of 776 discrete points that provide a grainy representation of the distribution of light within 3000 km s^{-1}. The outer shells become increasingly approximate because of the way the incompletion correction was made at discrete locations. Centaurus and Hydra I cluster points are *included* although they lie just beyond 3000 km s^{-1}. Those members of the two clusters with $V_0 < 3000$ km s^{-1} find there way into the NBG catalog. Rough corrections were made to account for the effect of the NBG velocity cutoff in deriving the light and positions associated with these two clusters.

Many of the discrete points in the map of the light distribution represent small groups or individual galaxies that have negligible influence. Ninety-seven percent of the light is in only 500 points with $\log L > 9.75 - 2 \log h$. Hence, we have ignored the points that are less luminous than this limit.

Yahil (1988), Strauss & Davis (1988), and Lynden-Bell & Lahav (1988) discuss stategies to account for sources lost in the zone of obscuration. Except in Ophiuchus and Orion, we should be quite complete at $|b| > 30°$ (about half the sky), but we must be quite *in*complete at $|b| < 20°$ (about a third of the sky). This uncertainty is substantial. As a warning, in our model the single greatest influence at our position, even with conservative corrections for obscuration, is the point associated with the low-latitude IC 342/Maffei group (group 14-11 in the NGB catalog). In our ultimately preferred model we actually do add *one* source in a region of high obscuration and not justified by what is seen. Also, a comparison model was developed that *does* include roughly the amount of matter

© American Astronomical Society • Provided by the NASA Astrophysics Data System

1992ApJ...391...16S

expected in the equatiorial band and we will discuss the implications of this case.

3.1. *Map Registration*

It is important that the map of the light distribution be reasonably well registered with the test particles with distances. The NBG atlas is based on observed velocities and a kinematic model: the Virgocentric flow model of Tully & Shaya (1984). To first-order, we will retain that model in our present map of the light distribution (appreciating that the zero-point to the distance scale is unimportant and everything can be scaled, for example, to a Virgo Cluster distance of unity). However, suppose that because of streaming with respect to the specific Virgocentric flow model, some filamentary structure in the light distribution map is mispositioned, such that the test particles with distances that are in reality drawn from that structure seem to be systematically displaced. Then the test particles would be thought to lie in a region where the model based on the light map anticipates a systematic flow toward the filament. In this hypothetical situation the test particles should be at rest with respect to this filament because they are well-mixed within it. This example illustrates why we require that the test particles and the light distribution maps be properly "registered."

The distance information can only be used to a limited degree for this purpose of registration. The sources in the light distribution map that correspond to the Virgo and Ursa Major clusters and only a few other nearby groups can be located by measured distances. However, the rms accuracy of 15%–20% in distance estimates is not sufficient in individual cases. At 3000 km s^{-1}, this uncertainty amounts to 450–600 km s^{-1}. By contrast, the narrowness of the filamentary structures in redshift suggest small-scale random motions must, in general, be less than 100 km s^{-1}. In other words, the light is more reliably located on small scales simply from velocities. Moreover, many of the sources in the light map have no distance estimates and *must* be located by their velocities.

Our procedure has been to begin with the Virgocentric kinematic model of Tully & Shaya (1984) scaled to our presently preferred zero point. The sources in the light distribution map associated with the Virgo and Ursa Major clusters are located by their measured distances. Similarly, for 10 groups in our local structure (the Coma-Sculptor Cloud: 14 in the NBG catalog) and for four other nearby groups, there is sufficient distance information to place the corresponding sources in the light map. Otherwise, the sample is separated into the "clouds" identified in the NBG catalog and if there are a sufficient number of distance estimates in a single cloud then a correction factor is found, such that, with this multiplier there is agreement in the mean between distances from the kinematic model and observed distances. Excluding the nearest 14 and 15 clouds, correction multipliers have rms excursions of 10% about unity. The corrections applied to 15 clouds are identified in Table 1. For other clouds there is insufficient independent distance information, and we strictly use the Virgocentric kinematic model. Overall there is good agreement between the adjusted kinematic distances and observed distances. The mean difference in distance modulus (measured – model) is -0.05 ± 0.51 (± 0.04) where the first uncertainty is the rms of individual measurements and the second uncertainty is the mean deviation for 142 groups and 53 single galaxies. The rms variation is due to the combination of distance measurement errors and departures from the adjusted kinematic model. Table 2 in TSP provides coordinates and fluxes associated with the discrete points that make up the map of the light distribution.

TABLE 1

CORRECTION MULTIPLIERS FOR INDIVIDUAL CLOUD DISTANCES

Cloud Name	Correction
11	0.89
12	0.90
13	1.01
14	1.44
15	1.51
21	0.93
22	0.85
41	0.76
42	0.99
44	0.99
51	1.03
52	1.03
53	1.13
61	0.98
71	0.86

NOTE.—Cloud names taken from "Nearby Galaxies Catalog."

NOTE.—Corrections applied to assure registration of mass centers with test galaxies.

3.2. *Mass beyond 3000 km s^{-1}*

Our map of the light distribution only extends to 3000 km s^{-1}. Beyond this volume, we assume the universe has constant density. Hence, our basic mass model has two free parameters. Inside a sphere of radius 3000 km s^{-1} there is mass at 500 discrete points defined by the light distribution and our free parameter is the mass-to-light (M/L) ratio [more accurately, as will be described next section, our free parameter is the product $(M/L)H_0^{-1}$]. Beyond 3000 km s^{-1}, our model requires our second free parameter, a uniform density characterized by $\Omega_0 = \rho_0/\rho_c$, the ratio of the mean density of the universe to the closure density.

A number of schemes could be contemplated for making the patch between the inner 3000 km s^{-1} region and the universe at large. The choice of M/L for the local sources and Ω_0 for the universe as a whole may be inconsistent, in the sense that there may be additional contributions to Ω_0 than the mass we associate with galaxies. We explore three possibilities which will be referred to as the one-, two-, and three-component models.

The one-component model will be used in the beginning. In this case, the only mass within 3000 km s^{-1} is that associated with the light by the selection of an M/L value. Hence with modest M/L choices and high values of Ω_0, the local region is underdense. In fact, this model can work well in low-density cases but not with high densities.

The two-component model, which is preferred, supposes that the global Ω_0 can be decomposed:

$$\Omega_0 = \Omega_{\rm smooth} + \Omega_{\rm gal}\,, \qquad (2)$$

where $\Omega_{\rm smooth}$ describes matter that is uniformly distributed or clustered only on extremely large scales and $\Omega_{\rm gal}$ describes matter clumped like the galaxies in our local sample. If the hypothetical $\Omega_{\rm smooth}$ exists, then it should permeate the local region. Hence, in our basic model we have a pedestal with $\Omega_{\rm smooth}$ throughout the region $V_0 < 3000$ km s^{-1} under the

© American Astronomical Society • Provided by the NASA Astrophysics Data System

1992ApJ...391...16S

discrete sources, while everywhere else the density is characterized by Ω_0. With our system of blue magnitudes (NBG catalog), the link between M/L and Ω_{gal} is given by

$$\Omega_{gal} \simeq (M/L)/(1600\ h) \quad (3)$$

(from Davis & Huchra 1982 with a 40% adjustment for our absorption corrections).

It is to be noted that the local region is not forced to have the mean density in this model. In fact, implicit in the Davis & Huchra (1982) calculation of the mean density there is excess luminosity nearby and that excess is preserved on top of the pedestal associated with the smooth component.

It will turn out that the two-component model provides as good a description as we have found, but a three-component model has been considered that, in the end, gave only upper limits on the degree of mass clustering on intermediate (i.e., 1–20 Mpc) scales. In this case, some fraction of the matter that makes up the global Ω_0 is placed in the vicinity of the 500 sources within 3000 km s^{-1} according to a recipe with an adjustable spatial scale factor. Details of this subsidiary model will be discussed in due course.

Finally, it might be the case that sources outside 3000 km s^{-1} have an influence on local motions. Our procedure was to see how well we could do without this added complexity and freedom and then to consider the additional influence of more distant sources. It will be discussed below why it was considered warranted to add three distant mass points.

4. CALCULATING PECULIAR MOTIONS

Our calculations are based on linear theory (Peebles 1980). The expected peculiar velocity of galaxy i is

$$\boldsymbol{v}_{pi} = [\delta g_i/(4\pi G\rho_0)]\Omega_0^{0.6}H_0 = (\tfrac{2}{3})\delta g_i \Omega_0^{-0.4}H_0^{-1} \quad (4)$$

where the *excess* gravitational acceleration $\delta \boldsymbol{g}_i$ is given by

$$\delta \boldsymbol{g}_i = \boldsymbol{g}_i - \boldsymbol{g}_{0i} \quad (5)$$

$$\boldsymbol{g}_i = -G \sum_{j\neq i}^{N} m_j(\boldsymbol{d}_j - \boldsymbol{d}_i)/|\,d_j - d_i|^3\ . \quad (6)$$

Here, $\boldsymbol{g}_i$ is the gravitational acceleration on the ith object due to $N = 500$ individual sources with masses m_j at separations $(\boldsymbol{d}_j - \boldsymbol{d}_i)$ but excluding the source that contains the ith object, while $\boldsymbol{g}_{0i}$ is the acceleration from a uniform density at the level of the mean density of the universe extending from the arbitrary center of the coordinate system (here, at the Local Group) to the position of the ith galaxy. Accordingly, at a position $\boldsymbol{d}_i$:

$$\boldsymbol{g}_{0i} = (-4\pi G/3)\rho_0 \boldsymbol{d}_i = -0.5\Omega_0 H_0^2 \boldsymbol{d}_i\ . \quad (7)$$

A constant density at distances greater than the galaxy's position from the center of the coordinate system has no gravitational effect. The geometrical construction of our model assures constant density with respect to the origin of our coordinate system on large scales. It can be seen that if there are *no* point sources then in the one-component model the "overdensity" within $\boldsymbol{d}_i$ is $-\rho_0$ and the effect of the mean density at large scales is a *repulsion*. This effect will be cancelled only when the density of galactic masses equals the mean density. As mentioned previously, we chose initially not to try to fill in the zone of avoidance with galaxies. However, to mitigate somewhat the artificial expansion resulting from a large empty zone, the expansion term $\boldsymbol{g}_{0i}$ was reduced by $\sim 17\%$. Otherwise the best fit might occur at a value of Ω that is slightly low.

The observed radial velocity, v_i, is the component of $\boldsymbol{v}_{pi}$, the peculiar velocity, along the direction from us to the galaxy minus the component of $\boldsymbol{v}_{LG}$, the Local Group peculiar velocity, along this direction plus the Hubble expansion velocity

$$v_i = (\boldsymbol{v}_{pi} - \boldsymbol{v}_{LG}) \cdot \hat{\boldsymbol{d}} + H_0 d\ . \quad (8)$$

The Local Group peculiar velocity is calculated by determining the acceleration on three galaxies: the Galaxy, M31, and M33 and then taking the luminosity-weighted average (M31, 49%; Galaxy plus Magellanic Clouds, 40%; M33, 11%).

It can happen that a test particle is located close to a source in the map of the light distribution, such that this source dominates the acceleration term for the particle. Hence, we do *not* calculate the acceleration on a galaxy due to the group that it is in and use the group velocity in place of the velocity of the individual system. Still, the test particle accidently might be located close to another accelerator. Also, there is the problem of the way the distance incompletion correction is applied at discrete locations. Consequently, it is clear that there can be spurious individual peculiar velocities associated with scales below a few megaparsecs.

4.1. *Free Parameters and Uncertainties*

Regarding the free parameters to our model, by combining equations (4)–(7) it is seen that the peculiar velocity arising from mass points depends on $(M/L)H_0^{-1}\Omega_0^{-0.4}$ and from the mean density depends on $\Omega_0^{0.6}H_0 d_i$. (The acceleration due to point masses depends on the choice of M/L but not H_0 because of the distance-square dependence of observed light.) Thus, in the basic model, there are only three parameters to vary: $(M/L)H_0^{-1}$, Ω_0, and $H_0 d_i$. In the latter product, the zero-point uncertainties in H_0 and d_i cancel out. The inclusion of mass points at large distances provides additional freedom. The *positions* and the *relative* masses of these sources are suggested by external information. There is a summary of the degree of freedom associated with the various "cases" that have been explored in Table 2.

TABLE 2

DEGREES OF FREEDOM FOR SIX CASES

Case	$H_0 d_{Virgo}$	Model	Standard of Rest	External Sources	ϕ (DOF)
0.....	1150	Hubble Flow	de Vaucouleurs	None	0
1.....	1150	M/L const	de Vaucouleurs	None	2
2.....	1370	M/L const	de Vaucouleurs	None	2
3.....	1370	(M/L const + uniform density)	de Vaucouleurs	None	2
4.....	1370	Same as 3	Peculiar LG motion	None	5
5.....	1370	Same as 3	Peculiar LG motion	GA	8
6.....	1370	Same as 3	Peculiar LG motion	GA, PP′, ShC	12

© American Astronomical Society • Provided by the NASA Astrophysics Data System

1992ApJ...391...16S

The choice of the local peculiar velocity introduces an uncertainty in equation (8). In our basic model we adopt the conventional correction for our motion of 300 km s^{-1} toward $l = 90$, $b = 0$ (de Vaucouleurs, de Vaucouleurs, & Corwin 1976). There are more recent evaluations (Yahil, Sandage, & Tammann 1977; Richter, Tammann, & Huchtmeier 1987). After a review, we concluded that the correction we make may not be the best but it is within the uncertainties and has the virtue of being standard. In the process of fine-tuning our model, allowance was made for the peculiar velocity of the local standard of rest beyond that implicit in the standard correction. Our fits could be slightly improved, as will be described.

It is becoming common to work in the rest frame implied by the microwave dipole (Lynden-Bell et al. 1988; Faber & Burstein 1988; Aaronson et al. 1989). Here, we work in a local rest frame. The difference is only a coordinate translation. Since all our objects with distances are so local, in the microwave background rest frame the dominant motion would be a common flow.

Then, there is an uncertainty in the value of H_0 that should be used in equation (8) to account for the universal expansion component of observed velocities. Here, the distance-scale zero point is irrelevant; at issue is the decomposition between peculiar and expansion velocities. In the basic one-component model, there is an interplay between the preferred value of H_0 and the overdensity associated with the Local Supercluster. If the overdensity is large, then objects that are observed within this same overdense region where we reside will tend individually to imply too low a value for H_0. The reason is that relative velocities tend to be retarded from the universal expansion in the overdense region (Tully 1988b).

Some ramifications will be mentioned when we compare the observations with models. The basic one-component model can compensate for a bad value of H_0 with an artificial value of Ω_0 (recalling that the interplay between M/L and Ω_0 can lead to spherical repulsion from a local underdensity or attraction from a local overdensity). From external considerations we prefer a value of $H_0 = 88$ km s^{-1} Mpc^{-1} with our zero point (Pierce & Tully 1988; Pierce 1989). As will be seen, this value results in a nice internal consistency. Note that the Great Attractor collaboration (Dressler et al. 1987; Lynden-Bell et al. 1988; Faber & Burstein 1988) effectively invoke the same external considerations when they take the Coma Cluster or the microwave background to provide the rest frame.

An evident concern must be the appropriateness of the linear approximation in an environment that includes the Virgo Cluster, among other density enhancements. This problem has been investigated by comparison with what we call "quasi-nonlinear" models. Yahil (1985) has introduced a term $(1 + \Delta\rho/\rho_0)^{-1/4}$ as a multiplier to equation (4) for peculiar velocities which is appropriate in cases of spherical symmetry and not extreme overdensity. In trial runs, we introduced this correction with each pairwise calculation of the influence of a perturber at the location of a test particle *if* the perturbation region is overdense. Here, ρ_0 is the mean density and $\Delta\rho$ is the excess density of the perturber at the position of the test particle. Evidently, in most cases the correction is insignificant. Comparison with the linear model results provides an indication of the limitations of the present procedures and can lead the way for fully nonlinear calculations (Peebles 1989, 1990). In practice, our pseudo-nonlinear models have *not* lead to improved fits. These trials suggest that the linear models are adequate for exploratory purposes.

5. A COMPARISON OF THE MODEL WITH OBSERVATIONS

Our basic model has only two free parameters: $(M/L)H_0^{-1}$ assigned to the 500 perturbers within 3000 km s^{-1}, and Ω_0 assigned to the uniform background. Consequently, when we began this study there was a quick answer to our zeroth-order question. *Yes*, there are reasonable values for the free parameters that generate a model velocity field with the general properties of the observed velocity field. That is, gravitational perturbations can produce the observed peculiar velocities. Most of the effort in the investigation, and space in the telling of the story, involves the exploration of reasonable limits on the parameter space and the potential effects of sources not in the basic model. In a sense, these are only details, albeit interesting details.

5.1. *Evaluation Techniques*

Specific models have been evaluated through a search for a minimum in a χ^2 parameter

$$\chi^2 = \sum_i^N n_i[(v_{i,\mathrm{ob}} - v_{i,\mathrm{th}})/H'_0\, d_i]^2 \ . \qquad (9)$$

Here, the ith test particle may be a group or an individual galaxy. The theoretical model predicts a radial velocity $v_{i,\mathrm{th}}$ at position $\boldsymbol{d}_i$, which can be compared with the observed radial velocity $v_{i,\mathrm{ob}}$ (group velocity, if appropriate). The distance d_i is determined by the TF method and, for groups, is averaged over n_i separate measurements. The parameter $H'_0 = H_0(1370/H_0\, d_{\mathrm{Virgo}})$, where d_{Virgo} is the distance to the Virgo Cluster, and renders the χ^2 values independent of the choice of H_0. The parameter χ^2 reduces to a measure of the observed minus model difference as a fractional uncertainty in distance by taking $[\chi^2/(\sum_i^N n_i - \varphi_{\mathrm{dof}})]^{1/2}$, where $\sum_i^N n_i = 265$ and φ_{dof} is the degrees of freedom in the model.

Our procedure was to plot grids of χ^2 values as a function of M/L and Ω_0, with the subsidiary parameters in more complex models held constant. For example, see Figure 1. A straight line corresponding to equation (3) is drawn on this and similar plots. In this region of the diagram, the value of Ω_0 is consistent with the proposition that all the mass is directly associated

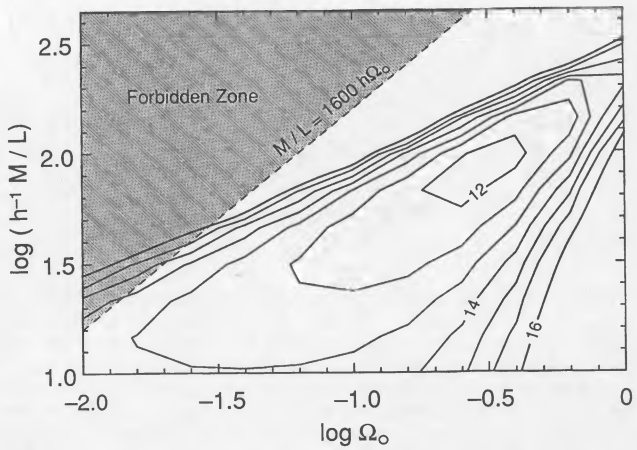

FIG. 1.—χ^2 contours in a M/L vs. Ω_0 plane for case 1 (one-component model, $H_0\, d_{\mathrm{Virgo}} = 1150$ km s^{-1} whence $H_0 = 74$ km s^{-1} Mpc^{-1} if $d_{\mathrm{Virgo}} = 15.6$ Mpc, de Vaucouleurs standard of rest). Minumum χ^2 of 12 reduces to an rms difference between $v_{i,\mathrm{obs}}$ and $v_{i,\mathrm{th}}$ of 21%. Contours of χ^2 values step in units of 0.7. The dashed line illustrates the case $\Omega_0 = \Omega_{\mathrm{gal}}$. The shaded region to the upper left of this line is excluded since $\Omega_0 \geq \Omega_{\mathrm{gal}}$.

© American Astronomical Society • Provided by the NASA Astrophysics Data System

1992ApJ...391...16S

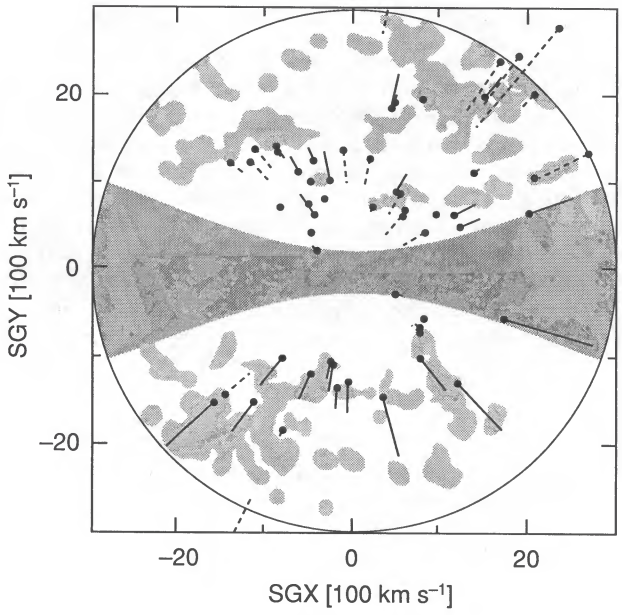

FIG. 2*a*

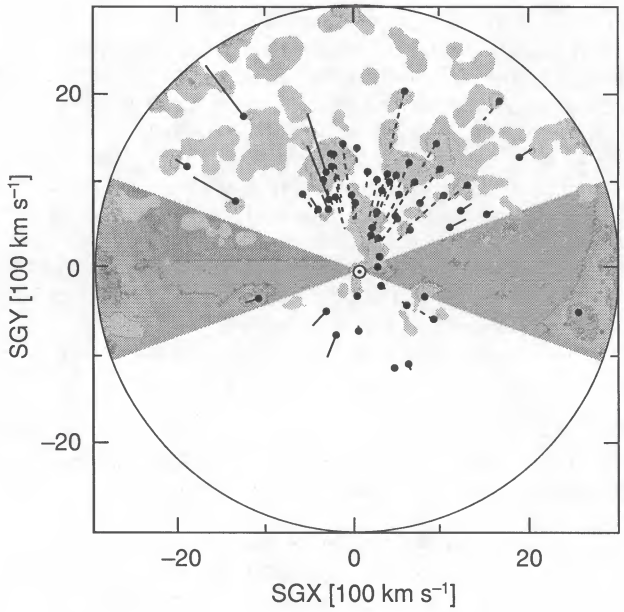

FIG. 2*b*

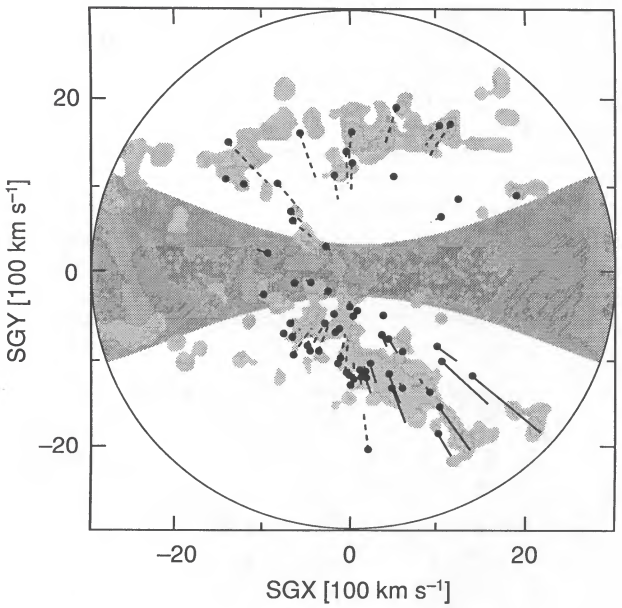

FIG. 2*c*

FIG. 2.—Observed velocities for galaxies with measured distances with $H_0 d_{\rm Virgo} = 1370$ km s^{-1} ($H_0 = 88$ km s^{-1} Mpc^{-1} if $d_{\rm Virgo} = 15.6$ Mpc). Supergalactic coordinates are used and the view is a projection onto the supergalactic equatorial plane. The filled circles represent the measured locations of galaxies (projections of $H_0 d_i$) and the end points of the solid or dashed lines represent the observed velocity (*solid lines* if $v_{i,\rm obs} > H_0 d_i$ and *dashed lines* if the contrary). Clouds of galaxies as represented in the NBG atlas are schematically superposed. The zone of obscuration is represented by the horizontal gray bands. (*a*) *Above* the plane of the Local Supercluster: members of the 40, 60, and most of the 70 series in the NBG catalog. (*b*) *In* the plane of the Local Supercluster: members of the 10 cloud series and a few from 70 series in the NBG catalog. Our location is indicated by the solar symbol. (*c*) *Below* the plane of the Local Supercluster: members of the 20, 30, and 50 cloud series in the NBG catalog.

with the light. The region in the diagram above and to the left of the straight line is excluded because the mass associated with the light implies a minimum value for Ω_0. A significant uncertainty is the accuracy of equation (3).

Another "tool" used for the evaluation of fits is point-by-point comparison of the theoretical and observed velocity fields. The object usually is to look for systematic effects, such as large regions where there is a systematic disagreement between the model and observations. Hence, we generate maps that locate the test particles at their measured distances (in velocity units) and extend radial vectors to the theoretical or observed velocities, or represent the difference between these, as appropriate. Radial vectors that point inward toward our position at the origin are dashed while radial vectors directed outward are solid. Displays of this type have been made popular by Dressler et al. (1987) and in subsequent work by the same colaborators.

There is the usual problem with projection effects when displaying a volume. Our experience with the "layering" of nearby galaxies parallel to the plane of the Local Supercluster leads us to display in three slices that project onto the so-called supergalactic equator. In Figure 2 and subsequent similar plots, panel (*a*) illustrates the region *above* the supergalactic plane, panel (*b*) illustrates the slice in this plane, and model (*c*) illustrates the region below the plane. The slices are not precisely defined in terms of supergalactic latitude because it was considered more important to preserve the integrity of filaments. Instead, *above* the plane includes all objects in clouds beginning with 4, 6, or 7 in the nomenclature introduced in the NBG catalog, *in* the plane includes objects in clouds beginning with 1, and *below* the plane includes objects in clouds beginning with 2, 3, and 5.

5.2. *Linear Calculations, No Distant Sources*

The first situation to be considered is the basic *one-component model* (i.e., no extra sources, conventional local rest frame) with H_0 set at 74 km s^{-1} Mpc^{-1} (called case 1). The χ^2 grid for this model is shown in Figure 1. It is seen that there are

© American Astronomical Society • Provided by the NASA Astrophysics Data System

1992ApJ...391...16S

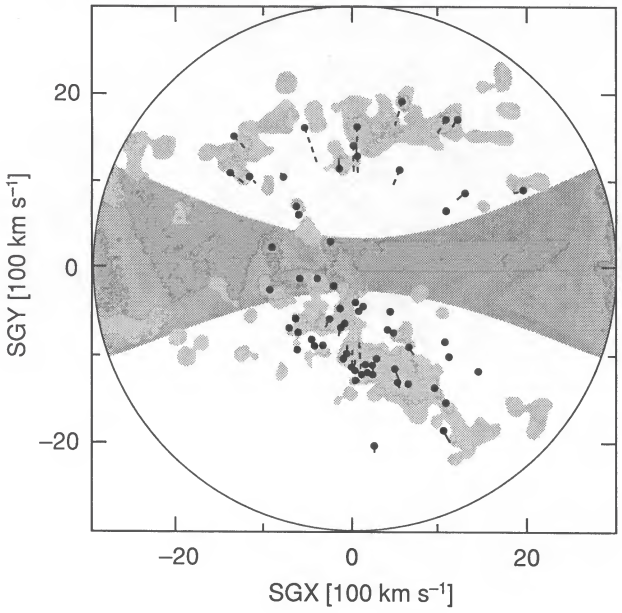

FIG. 3*a*

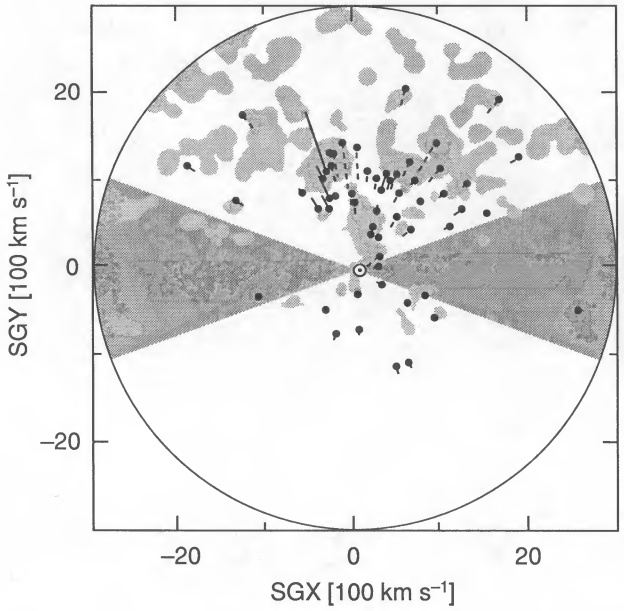

FIG. 3*b*

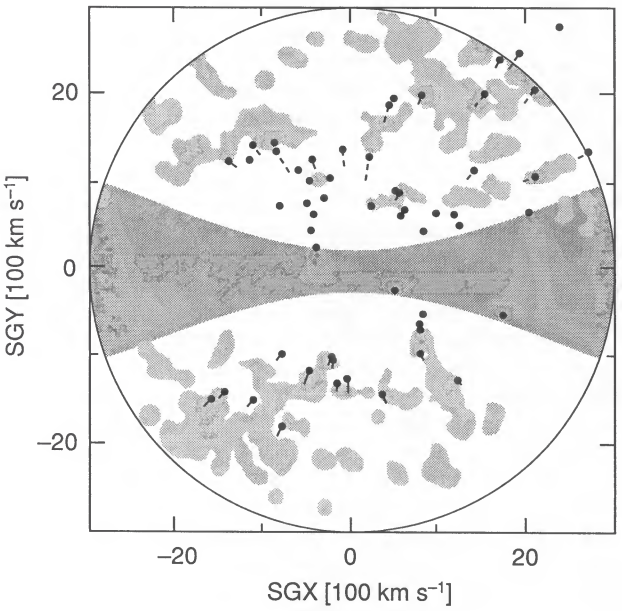

FIG. 3*c*

FIG. 3.—Modeled velocities for case 2 (one-component model, de Vaucouleurs standard of rest, $H_0 d_{\rm Virgo} = 1370$ km s^{-1}). Projections and slices as in FIG. 2. Filled circles again represent measured locations of galaxies ($H_0 d_i$ projections) and end points represent the velocities anticipated by the models.

elongated contours of constant χ^2 with a minimum M/L in the range 30–100 $M_\odot/L_\odot$. The fit is worse at small M/L values which, in the limit of $M/L = 0$, is equivalent to a pure Hubble flow model.

Before getting into detailed considerations of the fit, we want to dispatch with the particular problem of the choice of H_0. As was alluded to in a previous section, there is an interplay between the choice of H_0 and the preferred value of Ω_0 since varying either parameter changes the expected pattern of velocities in a spherically symmetric way with respect to our position. A low H_0 can be compensated by a high Ω_0. With our distance scale zero point, if one calculates the best value of H_0 under the assumption that there are *no streaming motions* (only random measurement errors and local peculiar velocities around pure Hubble expansion) then one is lead to H_0 in the mid to high 70's. A value in this range was assumed for case 1. However, in Figure 1 a preference is found for $M/L \sim 60$ $M_\odot/L_\odot$ which implies an *inconsistency* with the assumption of no streaming motions.

The effect of choosing a higher value of H_0 is that, in the mean, test particles have peculiar velocities that *point toward us.* This phenomenon is *a natural expectation if we live in an overdense region with a significant dynamical influence* (Tully 1988b). As to what we can say about H_0 from our data, we developed the impression from the one-component model that we had very poor internal constraints because of this possibility of trade-offs between H_0 and Ω_0. Consequently, we preferred to invoke external constraints on H_0 based on distance estimates for clusters with systemic velocities in the range 4000–11,000 km s^{-1} (Aaronson et al. 1986; Pierce 1989). On this basis, we choose $H_0 = 88$ km s^{-1} Mpc^{-1} if the distance-scale zero point is in accordance with $d_{\rm Virgo} = 15.6$ Mpc (whence $H_0 d_{\rm Virgo} = 1370$ km s^{-1}). In § 5.8, it will be shown that *self-consistency* with the two-component model actually requires H_0 to be close to this chosen value.

Case 2, then, is the same as case 1 except now $H_0 = 88$ km s^{-1} Mpc^{-1} is assumed. Figure 2 illustrates the pattern of *observed* peculiar velocities, projected onto the supergalactic plane, and Figure 3 shows the *theoretically expected* peculiar velocities, with $M/L = 48$ $M_\odot/L_\odot$ and $\Omega_0 = 0.03$. Figure 4*a* shows the χ^2 grid for this case, so one can see the motivation for these choices of M/L and Ω_0 (located by the large plus sign). The optimum χ^2 corresponds to 21% scatter in $|v_{i,\rm ob} - v_{i,\rm th}|$.

Before looking at Figures 2 and 3 in detail, we will make one last comment on the interplay between the choice of H_0 and Ω_0. It is seen in Figure 4*a* (and subsequent plots of this type) that the χ^2 residual contours are not closed at low Ω_0. This spurious result comes about because at low Ω_0, relatively high M/L models can provide the local overdensity required to

© American Astronomical Society • Provided by the NASA Astrophysics Data System

1992ApJ...391...16S

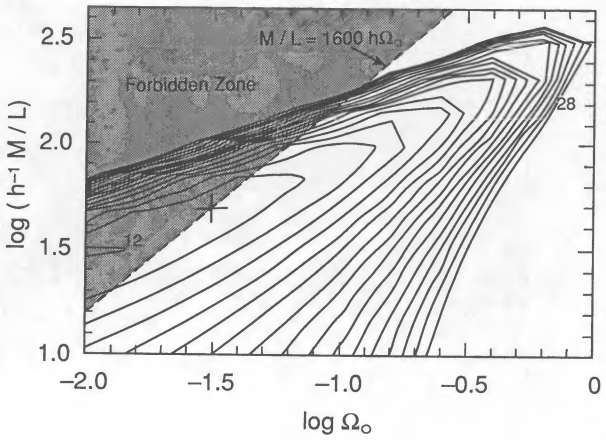

FIG. 4a

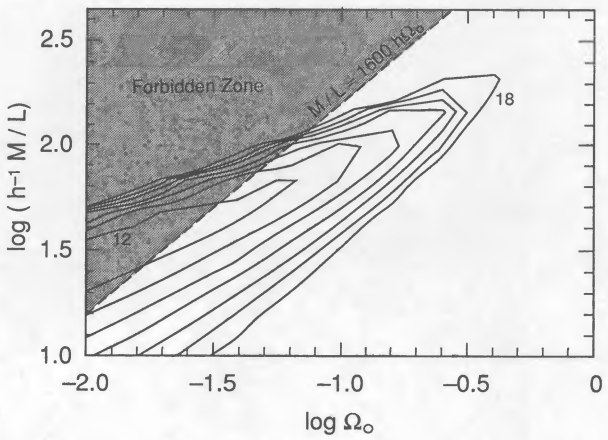

FIG. 4b

FIG. 4.—(*a*) χ^2 contours as a function of M/L and Ω_0 for case 2 (difference from case 1 is shift to $H_0\, d_{\rm Virgo} = 1370$ km s^{-1}). Minimum $\chi^2 = 12$. The region to the left of the $\Omega_0 = \Omega_{\rm gal}$ straight line is again excluded. The most favored one-parameter fit, indicated by a big plus, has $M/L \sim 50\, M_\odot/L_\odot$ and $\Omega_0 \sim \Omega_{\rm gal} \sim 0.03$. Above the trough of best fits there is a "wall" in the χ^2 domain: high M/L values can be excluded with a high degree of confidence. (*b*) χ^2 contours for case 2′ (difference from case 2 is addition of fake sources to the zone of obscuration). Minimum χ^2 is slightly improved but not significantly displaced.

describe the net inward peculiar velocities that comes about with $H_0 > 80$ km s^{-1} Mpc^{-1}. However, very low Ω_0 values can be excluded because the χ^2 minimum trough enters the forbidden zone above the diagonal line corresponding to $\Omega_{\rm gal} > \Omega_0$. From Figures 1 and 4 and subsequent similar figures, we derive *lower limits* of $\Omega_0 > 0.01$ and for the mass associated with the light map of $M/L > 15\ M_\odot/L_\odot$. These minimal values are consistent with the mass identified with galaxies within the domain of observed rotation curves.

A comparison of Figures 2 and 3 provides a qualitative feeling for the validity of the fit. Many features of the two maps are consistent, as is expected in view of the χ^2 minimization. Since this example is not the one we prefer, we will note only its three most evident *failures.*

One problem is in the immediate neighborhood of the Local Group where with any reasonable M/L value we get turnaround and the beginning of collapse involving the 14-10 (M81), 14-11 (Maffei/IC 342), and 14-12 (Local) groups. The dynamical importance of the Maffei/IC 342 Group at our position has also been noted by McCall (1989).

A second problem is the systematic outflow in the observed maps compared with the model maps in the region *below* the plane in the sector with SGX positive and SGY negative. The 51 and 52 clouds inhabit this region. The third problem is the systematic outflow in the observed compared with the model maps in a substantial fraction of the region *above* the plane.

5.3. *Effect of the Empty Zone of Obscuration*

As was mentioned in § 1, we have *not* generally attempted to account for mass that *must* exist in the zone of obscuration. Our reasoning has been that if we introduce spurious sources then we introduce spurious flows and we can never hope to recover information about what might actually lie in the Galactic plane. Indeed, our ultimate model *does* include an unseen source, but more about that later.

The referee feared that the artificial low-latitude void creates an uncertainty that placed in doubt the conclusions we will reach about M/L values and Ω_0. To answer those concerns we developed a model which did assign mass to the zone of obscuration and increased the expansion term g_{0l} to its full strength. Our recipe was to add point sources to the standard model by reflecting sources with $20 < |b| < 40$ into $0 < |b| < 20$. The $|b| > 20$ volume is slightly smaller than the $|b| < 20$ volume but, then, there are already *some* sources close to the plane in the standard 500 point model. It is a matter of taste, but we consider it a virture that the prescription provides for a clumpy distribution that retains some correlation with the large-scale clumpiness observed at high latitudes. This new model is called case 2′.

The χ^2 contours of case 2′ are shown in Figure 4*b*. In comparing these contours with those in Figure 4*a* of case 2, one sees that there is essentially no displacement of the overall grid. A noticeable improvement does occur in the lowest contour drawn $\chi^2 = 12$ which expands much farther across the minimum valley. This enlargement in input parameter space of the lowest contours probably occurs because case 2′ model does better represent reality than case 2.

The particular way we filled the zone of obscuration is arbitrary and can be faulted but the key point is that there was not much change. Unless some very extreme hidden mass distribution is entertained, our basic results about the character of the χ^2 domain on the M/L versus Ω_0 plots are likely to hold up. The fact that somewhat *lower* χ^2 values can be found with a model including mass in the zone of obscuration should not be a surprise. This model will not be our preferred one because it achieves the better fits at the expense of too many more degrees of freedom and ambiguities.

5.4. *Coupling between M/L and Ω_0*

If we pass to the *two-component model* with a constant density pedestal, there is a whole family of models that give indistinguishably good fits. It can be seen from equation (4) that similar peculiar velocities are generated by any model at fixed H_0 with $(M/L)\Omega_0^{-0.4} = constant$. Recall that the $\Omega_{\rm smooth}$ pesestal is chosen to make up the difference between $\Omega_{\rm gal}$ and Ω_0. We find a χ^2 minimum at

$$M/L = 140(H_0/88)\Omega_0^{0.4}\ . \qquad (10)$$

Hence, as one considers Ω_0 in the range from 0.02 to 1.0, the preferred M/L to associate with the galaxies in the light map varies from 30 to 140. This coupling is illustrated in Figure 5,

© American Astronomical Society • Provided by the NASA Astrophysics Data System

1992ApJ...391...16S

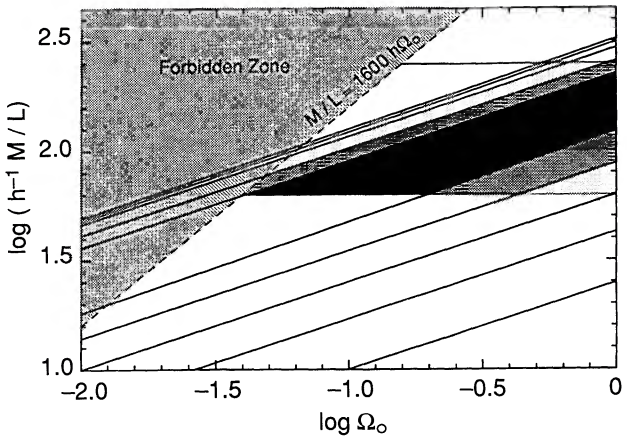

FIG. 5.—χ^2 contours as a function of M/L and Ω_0 for case 3 (difference from case 2 is addition of uniform density component). Now there is a minimum χ^2 trough along the line $M/L = 160\,h\Omega_0^{0.4}\,M_\odot/L_\odot$. The horizontal lines represent factor of 2 variances from the value $M/L = 125\,h\,M_\odot/L_\odot$ attributed in the mean to halos around individual galaxies from a virial analysis of groups. Within the considerable uncertainties, the group analysis provides a *lower limit* for M/L. Locations in the lower left corner of the shaded region are compatable with the proposition that all dark matter is in galaxy halos with scales of $\lesssim 300$ kpc while locations along the shaded portion of the trough at higher Ω_0 imply a contribution from a second, smooth component.

which is the χ^2 plot for the basic two-component model (case 3).

An equally low χ^2 can be found for any value of Ω_0 in the two-component model. If $\Omega_0 < 0.1$, within the uncertainties one has $\Omega_0 \sim \Omega_{gal}$, which is equivalent to a collapse to the one-component model. If $\Omega_0 > 0.1$ then a separate, smoothly distributed component is inferred. If $\Omega_0 \simeq 1$ then the smooth component dominates the clumped component of matter by an order of magnitude.

5.5. *Constraints on Intermediate-Scale Clustering*

There is an interesting conclusion to be drawn. The M/L values we require are about the same as values associated with galaxies on less than 1 Mpc scales. *Hence, there is no evidence for mass clustering on intermediate* (1–20 Mpc) *scales.*

This point is important enough to deserve amplification. Since the work by Zwicky (1933) and Smith (1936) there has been evidence for dark matter in clusters of galaxies, but these are special places in the universe. Flat rotation curves (Bosma & van der Kruit 1979; Rubin 1987) serve as evidence for dark matter in average galaxies, although information is limited to radii of only tens of kiloparsecs around the systems. The X-ray emission from coronae around early-type galaxies provides evidence of mass-to-light ratios of up to 100 $M_\odot/L_\odot$ in these special locations (Forman, Jones, & Tucker 1985). The presence of mass about typical galaxies on scales of several hundred kiloparsecs can be investigated by studying the kinematics of galaxy groups. For example, one of the best-known group compilations is by Huchra & Geller (1982; Geller & Huchra 1983). Taken at face value, the properties of these groups infer the existence of extensive dark matter halos about galaxies, but there are reservations about contamination of the group membership lists because of confusion or incompletion or velocity measurement errors or that the groups are not in a dynamical state that can be described by the virial theorem (Huchra & Geller 1982; Faber & Gallagher 1979; Byrd & Valtonen 1985).

We argue that these issues have been addressed and found not to be overwhelming in the group analysis by Tully (1987). Nearby groups are found to have homogeneous properties, with $M/L = 110(H_0/88)\ M_\odot/L_\odot \pm$ a factor 2 rms, on a scale characterized by the median virial radius of $290(88/H_0)$ kpc.

The groups that lead to this result lie within ~ 2000 km s^{-1} and, hence, are representative of the same region we are presently studying. These groups contain 77% of the light in the volume of the group analysis. The luminosity scale and corrections are the same in the earlier and present study. Hence, according to us *the conclusion is rather firm that, in the region of the Local Supercluster,* M/L-$110(H_0/88)$ *on scales of* ~ 0.3 Mpc. Translated to the universe at large, we conclude that $\Omega_{gal} = 0.08$ is the contribution to the mean density associated with mass clustered on a scale of 0.3 Mpc around luminous galaxies.

The group analysis limits provide the restriction indicated by the shading in Figure 5. It is seen to be entirely consistent with the results of the present study. Within the errors, M/L values inferred by our χ^2 fits agree with the group analysis values for $0.04 < \Omega_0 < 5$.

We introduce the *three-component model* in an attempt to constrain the influence of intermediate-scale clustering. Now the global Ω_0 will be taken to be the sum of a component discretely associated with galaxies, producing Ω_{gal}, a component peaked where there are galaxies but broadly distributed, producing Ω_{int} (for intermediate), and a component that is completely smooth, producing Ω_{smooth}.

A key assumption will be that the discrete component associated with galaxies has $M/L = 100\ M_\odot/L_\odot$, motivated by the group virial analysis results and, simultaneously, consistent with the two-component best fits. Since this choice is compatible with the best two-component model, we cannot expect the addition of intermediate-scale fluctuations to help, *and they do not help.* The point of the exercise is to see at what amplitudes and scales such fluctuations can be *excluded.* As amplitudes go to zero or scales go to infinity, it is equivalent to say Ω_{int} can be ignored.

The test is illustrated by Figure 6 which is a plot of χ^2 values

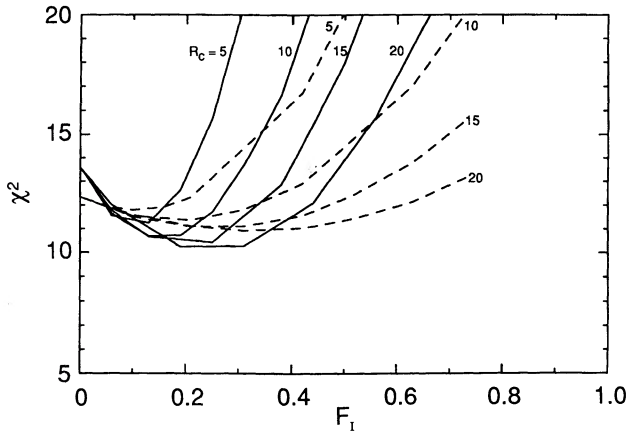

FIG. 6.—Effect of the intermediate-scale component on χ^2, for a three component model. The parameter

$$F_I = \Omega_{int}/(\Omega_{gal} + \Omega_{int} + \Omega_{smooth})$$

and Ω_{gal} is fixed by the choice $M/L = 100\,h\,M_\odot/L_\odot$. Solid curves correspond to various choices of the scale-length parameter R_c for the case $\Omega_0 = 1$, and dashed curves provide equivalent information if $\Omega_0 = 0.3$. Minimum χ^2 fits can only be achieved if Ω_{int} is small or $R_c \gg 20\ h$ Mpc, whence Ω_{int} becomes indistinguishable from Ω_{smooth}.

© American Astronomical Society • Provided by the NASA Astrophysics Data System

1992ApJ...391...16S

as a function of the parameter $F_I = \Omega_{\rm int}/\Omega_0$. The two cases that are explored have $\Omega_0 = 1$ (*solid curves*) and $\Omega_0 = 0.3$ (*dashed curves*). The additional parameter is a cutoff radius, R_c, which describes the *scale* of the intermediate fluctuations. Specifically, the mass associated with each of the discrete points in the one- and two-component models is augmented at a distance r from the point by the factor $F_I(\Omega_0/\Omega_{\rm gal})$ if $r > R_c$ or by $F_I(\Omega_0/\Omega_{\rm gal})(r/R_c)$ if $r < R_c$. This recipe is equivalent to an r^{-2} density fall off within R_c about each discrete source.

In Figure 6, it is seen that in a high-density universe ($\Omega_0 = 1$) there is little tolerance for fluctuations on intermediate scales. To get reasonable χ^2 with large F_I values one needs $R_c \gg 20$ Mpc which is equivalent to passing to the smooth approximation. In the $\Omega_0 = 0.3$ case, the fixed contribution from $\Omega_{\rm gal}$ is relatively more important, and there is more tolerance for intermediate-scale fluctuations. In any case, substantial intermediate-scale fluctuations inevitably degrade the fit.

Although we can say nothing about the possible existence of a uniform high-density background, it is concluded that the mass clustered on scales of less than 1 Mpc is at least comparable with mass clustered on scales of 1 Mpc or more and less than $\sim$20 Mpc. This result contradicts speculation that M/L might continue to grow on intermediate scales (Einasto, Kaasik, & Saar 1974; Ostriker, Peebles, & Yahil 1974). *Mass clustered on intermediate scales cannot come close to providing the density necessary for a closed universe in the standard model.*

5.6. *Tweaks on the Local Standard of Rest*

Up to this point, we have been using the usual local standard of rest advocated by de Vaucouleurs et al. (1976). A simple conversion to an alternative standard of rest proposed by Yahil, Sandage, & Tammann (1977) causes our χ^2 to *degrade* by 10%.

To explore the matter further, we allowed for an additional peculiar velocity of the Local Group in the χ^2 minimization. The three orthogonal components add 3 new degrees of freedom. The optimal fit is achieved with motions in supergalactic coordinates with respect to the de Vaucouleurs frame of $(-60, 40, -85) = 111$ km s^{-1} toward $\alpha = 9^{\rm h}38^{\rm m}$, $\delta = -31°$ ($l = 261$, $b = +16$). The χ^2, normalized by the increased degrees of freedom, *improves* by 11%.

This solution decribes the motion of the ensemble of the Local Group with respect to all the rest of our galaxies with distances, rather than the more familiar procedures which search for a rest frame with respect to galaxies in close proximity to the Local Group. At face value, our result hints at $\sim$100 km s^{-1} Local Group motion that cannot be explained by our model. Attractors in the zone of obscuration or departures from the linear approximation could account for this motion. The referee notes that the direction of this extra vector is close to the cosmic background dipole direction.

It is not suprising that the addition of free parameters leads to an improved fit. We conclude that the improvement is marginal and the basic model is not sensitive to the details of local motion. The "improved" local reference frame is incorporated in our final fits, but the difference with respect to the de Vaucouleurs standard is a minor subtlety. We will refer to this standard of rest (see Table 2) as "with peculiar Local Group motion."

5.7. *Distant Sources*

We cannot ignore the evidence already described in § 1 for long-range gravitational influences. On the other hand, there is no detailed information at our disposal on the distribution of galaxies beyond 3000 km s^{-1}. Our compromise has been to add the fewest possible sources at large distances, guided by external information such as the *IRAS* maps (e.g., Yahil 1988) and the literature on the Great Attractor (e.g., Lynden-Bell et al. 1988; Faber & Burstein 1988). Our constraints are the χ^2 *fits* and the degree of agreement with *the motion inferred from the microwave background dipole.* It will be described how we can get good results with just three distant sources.

Our first extra source (case 5) represented the "Great Attractor" (GA) and was initially located at the position recommended by Faber & Burstein (1988). We allowed ourselves the freedom to define the mass of this source. The optimum χ^2 dropped 10%, accounting for the extra degrees of freedom in the normalization. The systematic streaming associated with clouds 51 and 52 and above the supergalactic plane is reduced but not eliminated. Interestingly, the problem in the vicinity of the Local Group is nicely solved. *The tidal action of the Great Attractor is enough to stall the general collapse of the nearest several groups.* This effect is a curious example of the influence of large-scale tidal forces of the sort that we have mentioned in several papers (see Shaya & Tully 1984). With a mass of $2 \times 10^{16}\Omega_0^{0.4}\ M_\odot$, the model predicts a motion of 353 km s^{-1} toward SGL = 143, SGB = -21, compared with the motion inferred from the microwave dipole of 615 km s^{-1} toward SGL = 137, SGB = -37.

In spite of this reasonable agreement with the dipole motion, if we are to be guided by the *IRAS* maps (Yahil 1988) then there must be more to the story. Simply judging by the relative numbers of *IRAS* sources and their distances, the Perseus-Pisces region could be expected to have $\sim$40% of the gravitational influence of the Great Attractor.

As an initial complication to the GA model, we placed a mass point at a location indicated by the concentration of *IRAS* sources in Perseus-Pisces (PP) and set $\log L_{\rm PP} = \log L_{\rm GA} - 0.2$ in accordance with the relative prominence of the two regions in the *IRAS* maps. However, the χ^2 was not improved significantly, and we subsequently realized that the reason is because PP and GA are almost antipodal. Long-range gravitational forces have symmetric effects at the antipods and can hardly be distinguished. The major effect of introducing PP was to destroy the rough agreement with the motion inferred by the microwave background dipole since PP largely offsets GA. This dilemma with regard to Perseus-Pisces has related manifestations that were noted by Dekel & Berstchinger (1990).

It was Dekel & Bertschinger who gave us a hint of how to improve our model because they noted that the most apparent *disagreement* between their map of the local mass distribution and the NBG atlas was what they called the "mystery peak." In fact, this region is in the direction of high Galactic latitude obscuration in Orion and only 30° or so from PP. Hence, we allowed the projected location of PP to float and, sure enough, we obtained better χ^2 fits when PP was moved over to the region of the Dekel-Bertschinger "mystery peak" and, in fact, somewhat beyond, to the Galactic anticenter region (we will refer to this "displaced" PP source as PP′). The best χ^2 fit was improved a further 13%, corresponding now to 18% in the observed minus model velocity difference. There was still the problem with the microwave background since PP′ and GA are still roughly on opposite sides of the sky. To accommodate that constraint with only these two distant sources we could flip the revised PP′ source to its antipodal location near the Galactic Center!

© American Astronomical Society • Provided by the NASA Astrophysics Data System

1992ApJ...391...16S

Before arriving at our preferred model, we will take an excursion and say why we *do not* include the next most obvious long-range source: the Coma Cluster and its surroundings. The previously mentioned sources provide a desired stretch along an axis between the Great Attractor and Perseus-Pisces regions and compression orthogonal to this axis. Coma tends to stretch where we want compression. If we place a source at the location of Coma we end up with an *upper* limit of $\log (M_{\rm coma}/M_\odot) < 15.5\Omega_0^{0.4}$ which is hardly more than we know exists in the Coma Cluster itself.

Finally, we will discuss our preferred placement of the long-range forces, to be called case 6. Our main problem with the two source (GA + PP′) solution is the disagreement with the microwave background dipole unless the concentration of objects in Perseus-Pisces is a ruse and there is an unsuspected concentration behind the Galactic center, near the PP′ antipod.

We were propelled toward our final solution when we saw unpublished maps by R. Scaramella, G. Vettolani, & G. Zamorani (private communication) of the combined distribution of Abell (1958) and Abell, Corwin, & Olowin (1989) galaxy clusters. Scaramella et al. (1989) had already drawn attention to a concentration of rich clusters at 14,000 km s^{-1} behind the "Great Attractor" region and the new maps reveal that there are 5 times as many rich clusters as in GA, at $\sim$3.7 times the distance. It is clearly the dominant high-density region on the cluster maps and, from a consideration of the relative number of clusters, could have 30%–40% of the gravitational influence of the Great Attractor (Scaramella, Vettolani, & Zamorani 1991; Plionis & Valdarnini 1991). Lahav et al. (1989) have noted a concentration of X-ray sources, Raychaudhury (1989) has found an excess of galaxies in a survey with UK Schmidt plates that extend to $B_J = 17^{\rm m}$, and Allen et al. (1990) have seen an excess of luminous *IRAS* galaxies all in the same region behind the Great Attractor. Remarkably, Shapley (1930) saw evidence for the same excess peaked at $m_{\rm pg} \sim 17^{\rm m}.4$ on long-exposure Bruce plates. We follow Raychaudhury and refer to the region as the "Shapley Concentration" (ShC).

From the information in the clusters map, we chose a position and distance for the ShC source and distances for the GA and PP′ sources (GA is moved closer by 12% from the Faber-Burstein position to give better agreement with what is seen in the clusters map). The three long-range sources, GA, PP′, and ShC) were allowed to vary in strength and GA and PP′ could float in position until an optimum solution was achieved. The parameters of the long-range sources are given in Table 3. Figure 7 demonstrates the χ^2 sensitivity to the strengths of the three sources and Figures 8 and 9 show the constraints on the plane of the sky. The Shapley Concentration source offers negligible improvement to the χ^2 fit (since it is in the same direction as GA) but solves the problem of the microwave dipole. The best χ^2 fit still gives 18% observed − model velocity differences. Model velocity vectors for the "preferred" model are shown in Figure 10. The comparable map of observed velocities is Figure 2 and the *difference* vectors are shown in Figure 11. The χ^2 minimum trough in the two-parameter model is now

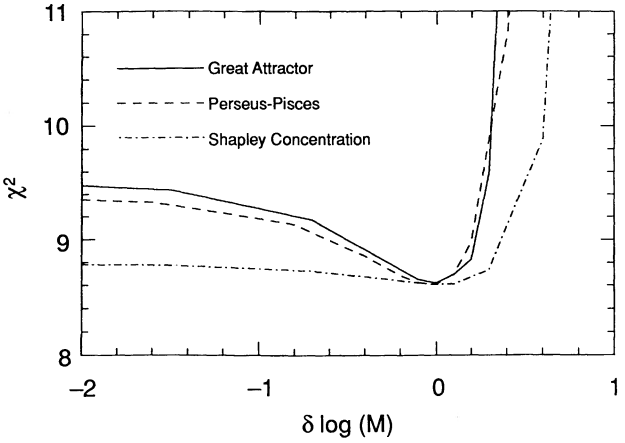

FIG. 7.—Effect of varying the masses of the external sources on χ^2. Positions are fixed. One mass is varied while the others are held at their optimal values.

$$M/L = 127(H_0/88)\Omega_0^{0.4}\,. \qquad (11)$$

The $\sim$10% reduction in M/L values compared with equation (10) arises because long-range tidal forces from the distant sources replace the need for local mass to a degree.

There are still seen to be some residual streaming motions unexplained by our final model. There are outward motions below the plane in the sector SGX > 0, SGY < 0 which are actually *worse* in our final model than they were with a model involving a source at the *nondisplaced* PP. Also, there are general outward motions yet to be explained in the "above the plane" map. It is almost certain that we could explain these problems with the judicious placement of a couple of additional sources but the solutions would not be unique and the relative simplicity of our current model would be somewhat compromised. Clearly, there is room for improvement.

In the cosmic microwave background rest frame, our model gives a Galactic motion of (−282, 301, −367) = 552 km s^{-1} toward $\alpha = 10^{\rm h}18^{\rm m}$, $\delta = -23°$ or $l = 263°$, $b = +28°$ or SGL = 133°, SGB = −42°. Figure 12 illustrates the separation of this peculiar motion according to all the contributions in our model. If the local motion not anticipated by the model is included then the global Local Group motion is 661 km s^{-1} into SGL = 135°, SGB = −43°. Among the sources within 3000 km s^{-1}, the one with the greatest influence is group 14-11 (Maffei/IC 342) with a contribution of 52 km s^{-1}. The Virgo Cluster (group 11-1) alone has accelerated us by only 29 km s^{-1}! It is to be appreciated that this result is obtained with the same M/L value assigned to all components. A more sophisti-

TABLE 3

PARAMETERS OF THE THREE EXTERNAL SOURCES

Source	Mass ($\Omega_0^{0.4}10^{16}\,M_\odot$)	$H_0 d$ (km s^{-1})	α	δ	l	b	SGL	SGB
Great Attractor	1.5	3700	$14^{\rm h}40^{\rm m}$	−47	321	11	169	5
Displaced Perseus-Pisces	5	5460	$5^{\rm h}52^{\rm m}$	10	197	−8	355	−60
Shapley Concentration	26	13800	$13^{\rm h}28^{\rm m}$	−31	312	31	149	−1

NOTE.—Distances set by positions of concentrations on *IRAS* galaxy survey and rich cluster maps.

© American Astronomical Society • Provided by the NASA Astrophysics Data System

1992ApJ...391...16S

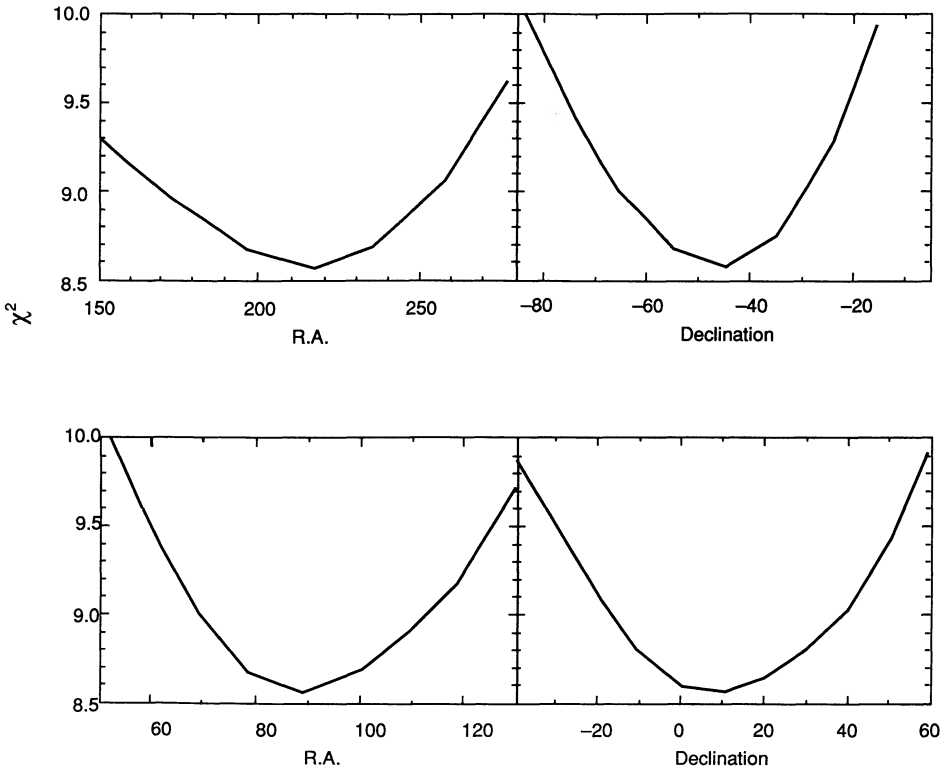

FIG. 8.—Effect of varying the positions of the external sources on χ^2. Masses and distances are fixed. (*a*) Effect of varying right ascension of GA only. (*b*) Effect of varying declination of GA only. (*c*) Effect of varying right ascension of PP′ only. (*d*) Effect of varying declination of PP′ only. Minimum value of $\chi^2 = 8.6$ corresponds to a normalized difference $(v_{i,\mathrm{obs}} - v_{i,\mathrm{th}})$ of $\pm 18\%$ in distance.

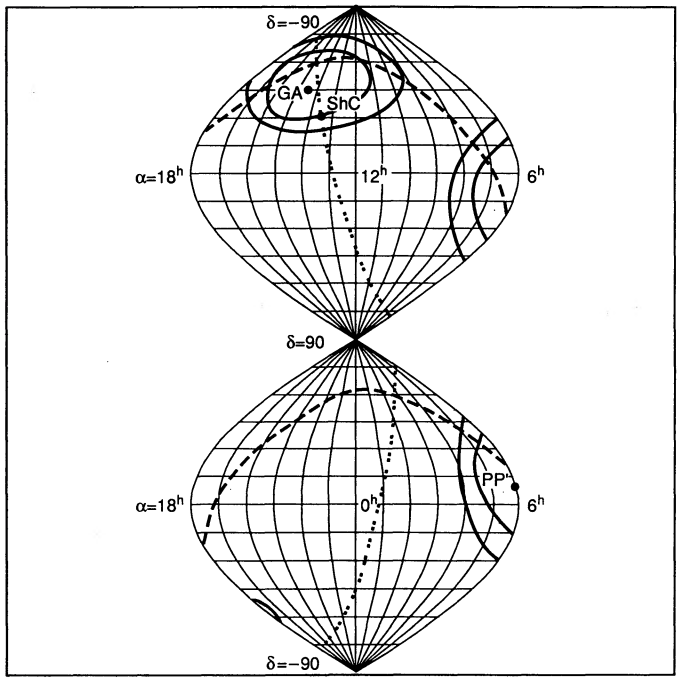

FIG. 9.—Contours of constant χ^2 projected onto the sky illustrate the delineation of the GA and PP′ source locations. ShC is positioned on the concentration of clusters at 13,800 km s^{-1}. The Galactic and supergalactic equators are identified by the dashed and dotted curves, respectively.

cated nonlinear calculation might accommodate a higher M/L value in a special region like the Virgo Cluster and, hence, result in a greater influence.

The three distant sources all have comparable influence. The sources GA + ShC are partially offset by PP′ to produce the observed supergalactic plane component of our motion with respect to the microwave background rest frame and, surprise, the PP′ source serves to explain the component of motion orthogonal to the plane! Of course, our model beyond 3000 km s^{-1} is too simplistic.

Interestingly, Willick (1990) has studied flows in the Perseus-Pisces region and finds an overall flow of -450 km s^{-1} toward us and the microwave dipole direction. He argues that this large-scale coherence with our own motion of ~ 600 km s^{-1} in the same direction cannot be entirely explained by a mass concentration as close as the Great Attractor. He concludes that the streaming coherence length is of order 10,000 km s^{-1}. We note that the distance from ShC to PP actually corresponds to more like 20,000 km s^{-1}.

5.8. *M/L of Distant Sources*

There are *hints* that M/L values associated with the distant sources are higher than in the local region by a factor in the range 3–10. Here are two arguments.

The first requires an approximation of the light associated with the GA and ShC regions. In ShC, there are 29 rich clusters in a projected radius of $57(88/H_0)$ Mpc, or a "domain" of $19(88/H_0)$ Mpc per cluster. In our map of the Local Super-

© American Astronomical Society • Provided by the NASA Astrophysics Data System

1992ApJ...391...16S

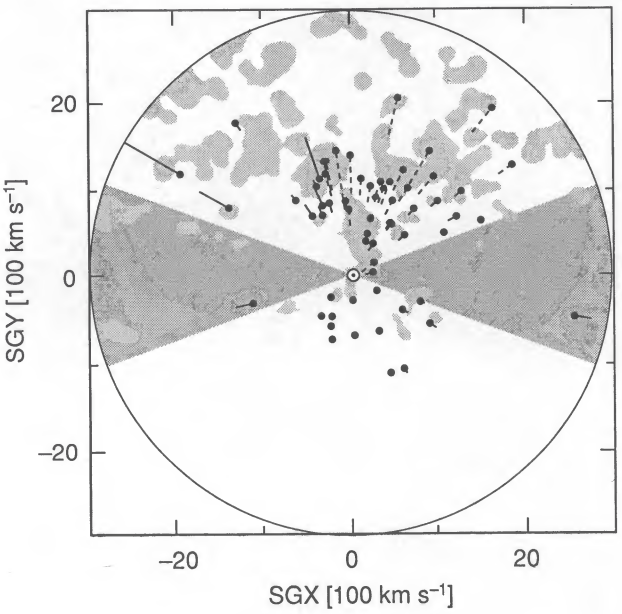

FIG. 10*a*

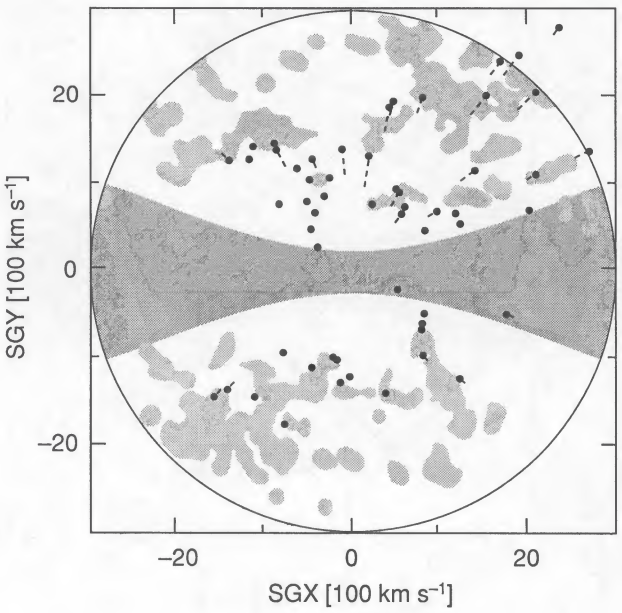

FIG. 10*b*

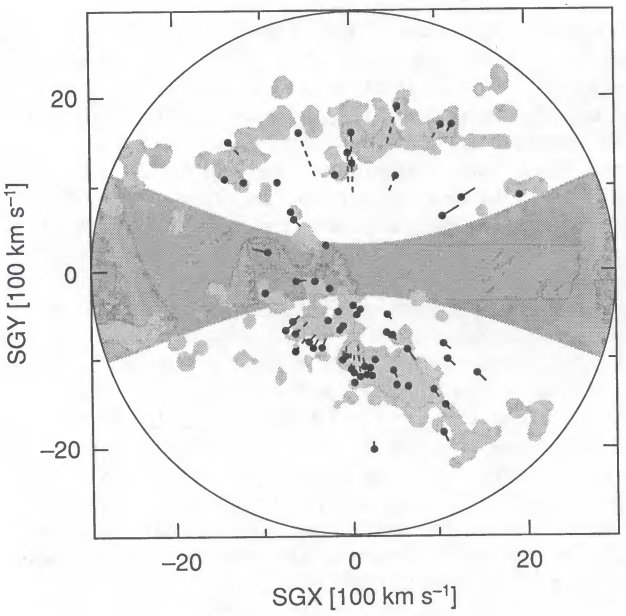

FIG. 10*c*

FIG. 10.—Modeled velocities for case 6 (two-parameter model, with peculiar LG motion, $H_0 d_{\rm Virgo} = 1370$ km s^{-1} whence $H_0 = 88$ km s^{-1} Mpc^{-1} if $d_{\rm Virgo} = 15.6$ Mpc, and GA, PP′, and ShC external sources). Symbols, projections, and slices are the same as for Fig. 3.

cluster region, there is $1.00 \times 10^{13}\ L_\odot$ within an equivalent domain around the Virgo Cluster. If we make the incredibly naive assumption that the light within each rich cluster "domain" is similar to the equivalent domain around Virgo then we except $3 \times 10^{14}\ L_\odot$ in ShC. The "expected" mass of $127(H_0/88)\Omega_0^{0.4} \times 3 \times 10^{14}\ M_\odot$ can be compared with the required mass given in Table 3. The implication is a seven-fold enhancement of M/L over the local region. Similarly, in GA there are seven clusters in a radius of $20(88/H_0)$ Mpc, or a "domain" of $11(88/H_0)$ per cluster. Within such a radius around Virgo there is $0.53 \times 10^{13}\ L_\odot$, whence the expectation in GA is $4 \times 10^{13}\ L_\odot$. The M/L enhancement required over the local region is a factor of 9.

The second argument comes from galaxy counts. Lynden-Bell & Lahav (1988) considered galaxy catalogs that extend to the GA region, though not as deep as ShC. They found a dipole in the galaxy distribution that agrees in direction with GA but apparently not in amplitude. With an assumption of constant M/L, there would be a shortfall of mass compared with the microwave dipole requirement. Similarly, Raychaudhury (1989) finds an excess of galaxies in the ShC region compared with a control area but, once again, concludes that although the direction is coincident with the microwave dipole, the amplitude of the light enhancement is insufficient.

With each of these arguments, it is difficult to evaluate the volume one should be attributing to the enhancement and a factor of 2 linear uncertainty translates to an order of magnitude in the volume. Then there is the obvious wild card of the zone of obscuration which is so close to the GA and ShC lines of sight. This factor prevents us from any speculation about PP′. Also, our three distant sources model is hopelessly simple.

We dare to mention this hint of a mass-per-galaxy or mass-per-volume variance because it is important to clarify. Occum's razor would favor that there be only *one* kind of mysterious dark matter: whatever it is that gives $M/L \sim 100\ M_\odot/L_\odot$ and is concentrated on scales smaller than 1 Mpc around galaxies. The "cold dark matter" model (Blumenthal et al. 1984; White et al. 1987) provides a scenario for picturing this circumstance. On the other hand, there is growing evidence for structure on extremely large scales, now reinforced by the map by Scaramella et al. and the evidence for large-scale mass variation is tantalizing. There could be a slowly varying "hot" component. Alternatively, an intriguing possibility is suggested by the "hybrid" model by Blumenthal, Dekel, & Primack (1988), where it was proposed there could be comparable $\Omega_0 \sim 0.1$ contributions from cold dark matter and from baryons clustered on the $10^{17-18}\ M_\odot$ scale of the light-travel horizon at the epoch of recombination. In this latter case, presumably most

© American Astronomical Society • Provided by the NASA Astrophysics Data System

1992ApJ...391...16S

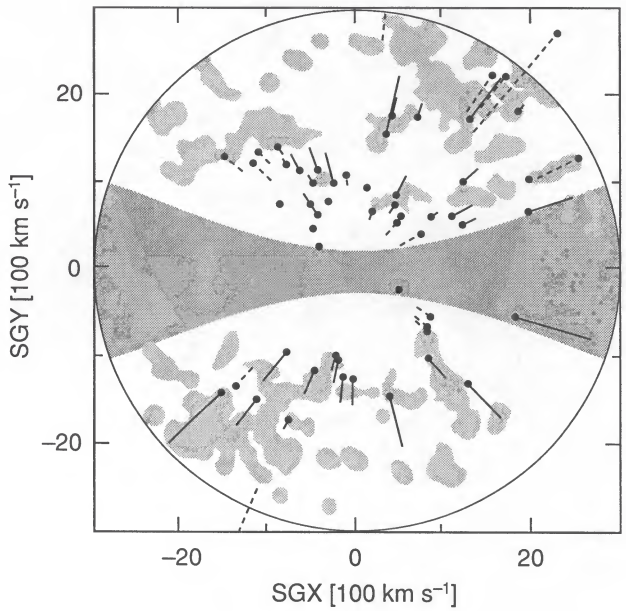

FIG. 11*a*

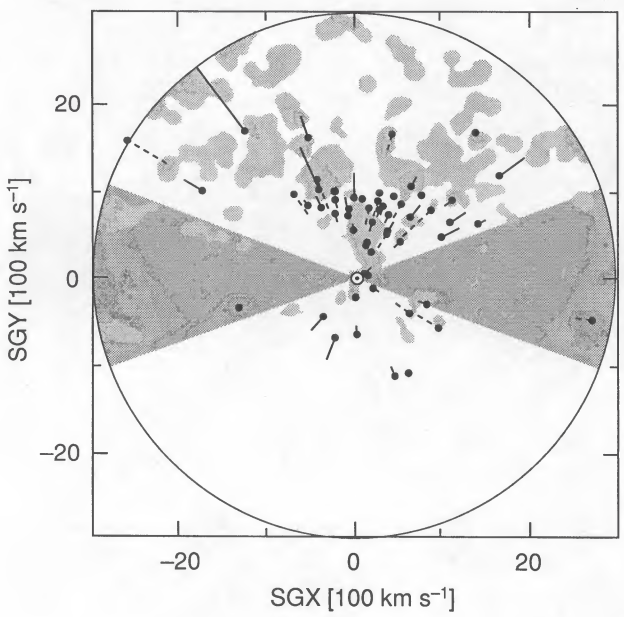

FIG. 11*b*

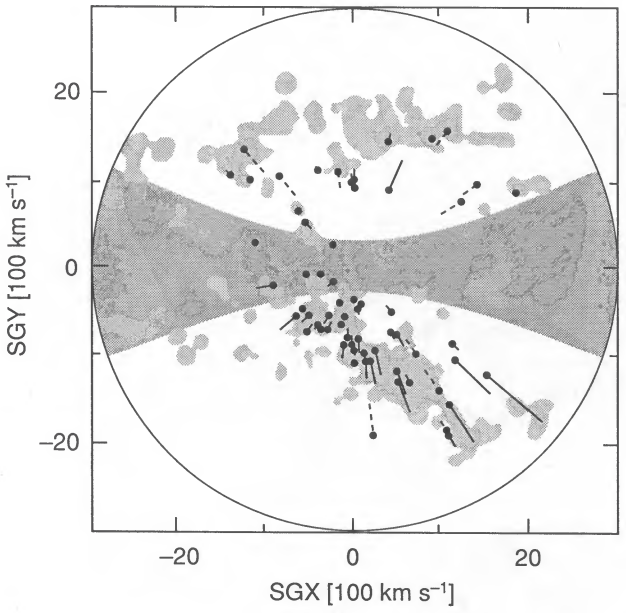

FIG. 11*c*

FIG. 11.—Observed minus modeled velocity differences for case 6. Vectors are essentially the differences between the vector end points in Figs. 2 and 10 (except now with peculiar LG motion for both). *Solid line:* $v_{i,\mathrm{obs}} > v_{i,\mathrm{th}}$; *dashed line:* $v_{i,\mathrm{obs}} < v_{i,\mathrm{th}}$; *dotted line:* $v_{i,\mathrm{obs}} \simeq v_{i,\mathrm{th}}$.

matter has condensed into small-scale knots but the ratio of baryons to dark matter might vary on large scales.

5.9. *Confirmation of the Choice of H_0*

The value $H_0 = 88$ km s^{-1} Mpc^{-1} (or $H_0\, d_{\mathrm{Virgo}} = 1370$ km s^{-1}) has been used because of external considerations: the distances and velocities of clusters at substantial redshifts. It eventually dawned on us that the two-component model does not allow a trade-off between H_0 and Ω_0 because the pedestal provided by Ω_{smooth} removes the artifact of an exaggerated local hole or excess which could simulate a radial flow pattern. Equivalently, we can speak of a *constrained* one-parameter model where Ω_0 is required to equal Ω_{gal}. The introduction of the second parameter with Ω_{smooth} just allows for the discussion to be extended to a family of equally good solutions.

We found that optimum fits were given for well-defined values of H_0. In the case of no sources external to 3000 km s^{-1} our best value is $H_0 = 83$ km s^{-1} Mpc^{-1}, while with the preferred model with three external sources the best value of H_0 is increased to 88 km s^{-1} Mpc^{-1}. The χ^2 domain is illustrated in Figure 13 for this latter case. Happily, the optimum value of $H_0\, d_{\mathrm{Virgo}}$ is just what we have been using and this circumstance is a strong conformation of the validity of our choice. The best fit corresponds to $\Omega_0 = \Omega_{\mathrm{gal}} = 0.02$, consistent with the two-parameter result: $M/L = 144\ h\Omega_0^{0.4}$. Again, the zero point is *not* being tested and can be arbitrarily changed. We persist in using the specific value associated with the choice $d_{\mathrm{Virgo}} = 15.6$ Mpc because if the reader accepts that we can measure individual distances well enough to map peculiar velocities then (s)he might entertain that we can do the simpler job of establishing the zero point (Pierce & Tully 1988, 1991).

The χ^2 trough toward low Ω_{gal} in Figure 13 is due to the trade-off possibilities between M/L and H_0 (recall discussion in § 4.1). The line at $\Omega_{\mathrm{gal}} = 0.008$ corresponds to $M/L = 12\ h\ M_\odot/L_\odot$, the rather firm lower limit provided by the mass associated with individual galaxies from rotation curve information (see Bosma & van der Kruit 1979).

5.10. *The Local Velocity Anomaly*

Part of the historical debate regarding the Hubble Constant has gone around on whether or not there is a significant departure from universal expansion velocities in the local vicinity. De Vaucouleurs (1958) was an early champion of this idea, although Bottinelli et al. (1986) and Kraan-Korteweg, Cameron, & Tammann (1986), among others, have argued for the alternative hypothesis of Malmquist bias. The matter has most recently been discussed by Tully (1988b, d), Faber & Burstein (1988), Giraud (1990), and Han & Mould (1990).

© American Astronomical Society • Provided by the NASA Astrophysics Data System

1992ApJ...391...16S

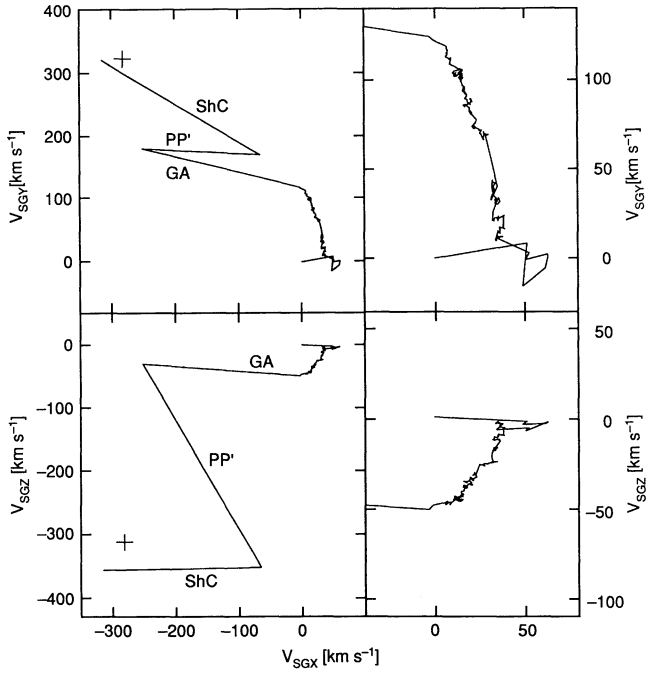

FIG. 12.—Decomposition of the local peculiar velocity vector. Each of the 500 sources within 3000 km s^{-1} and three sources beyond this distance contribute to the overall peculiar velocity of the Local Group. *Upper right panel:* vector sum of the contributions by the inner 500 sources projected onto the SGX–SGY plane. *Upper left:* all sources, SGX–SGY projection. *Lower right:* inner 500 sources, SGX–SGZ projection. *Lower left:* all sources, SGX–SGZ projection.

Our preferred model provides a reasonably pleasing description of observed motions in the region of the local anomaly. This side issue is discussed in TSP, where several sequences of figures are presented illustrating the degree of fit. The essential point is that $2 \times 10^{14}\Omega_0^{0.4}$ $M_\odot$ within our Coma-Sculptor Cloud and the neighboring Leo Spur have caused some local deceleration. Tidal compression from distant sources is also a factor.

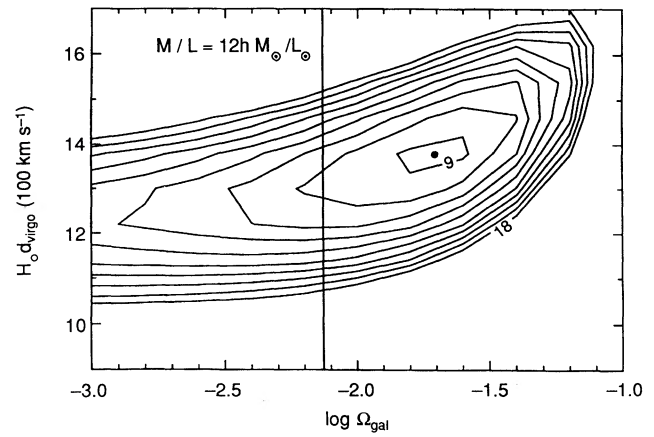

FIG. 13.—Confirmation of the choice of H_0. The χ^2 contours in the $H_0 d_{Virgo}$ vs. Ω_{gal} plane for a constrained one-component model ($\Omega_0 = \Omega_{gal}$) which has the three external sources and, hence, is a special case of the case 6 model. Minimum χ^2 occurs for $H_0 d_{Virgo} = 1370$ km s^{-1}, whence $H_0 = 88$ km s^{-1} Mpc^{-1} if $d_{Virgo} = 15.6$ Mpc. The preferred value of $\Omega_{gal} = 0.02$ is consistent with the best two-component model with $M/L = 144\, h\Omega_0^{0.4}$. The vertical line corresponds to a rather firm lower limit given by $M/L = 12\, h\, M_\odot/L_\odot$ from galaxy rotation curves.

6. SUMMARY

1. A gravity field associated with matter distributed like the observed galaxies will generate a velocity field very much like what is observed locally. The similarity is too good to be a coincidence. The conclusion must be that mass is basically distributed like the light and peculiar velocities are basically generated by gravitational perturbations. Yahil (1988) and Dekel & Bertschinger (1990) had already reached this same conclusion.

2. A surprisingly compelling result of this study comes from the coincidence between the preferred M/L value found from our modeling of galaxy flows and the M/L value that is given by a detailed group analysis (Tully 1987). The group analysis implies $M/L \sim 100\ M_\odot/L_\odot$ on scales smaller than 1 Mpc around individual galaxies. The present supercluster analysis implies there is *not significantly* more mass associated with these same galaxies clumped on scales up to $\sim$20 Mpc. Han & Mould (1990) reach a contradictory conclusion but our analysis is more direct and probably more sensitive. The good agreement between observations and our model is *completely destroyed* if matter clumped on scales of 20 Mpc or smaller corresponds to M/L values greater than $\sim 200\ M_\odot/L_\odot$. The χ^2 *wall* at high M/L values is to be noted in Figure 4*a* and related figures. The inferrence is $\Omega_{gal} \sim 0.03$–0.1 associated with matter clustered on scales of 20 Mpc or smaller. If Ω_0 is significantly larger, say $\Omega_0 \sim 1$ as often preferred, then the extra required dark matter has *nothing to do with* the dark matter that resides in galactic halos. The evidence is speculative whether this second form of dark matter exists and the simplest hypothesis is that it does not exist.

3. The inferrences from the placement of the distant sources is interesting but more uncertain. Of course, the use of only three sources represents a gross oversimplification and the details of our representation are not very noteworthy. In particular, it can be assumed that the PP′ source adopted the position it did because a source near the Great Attractor antipod is not too helpful for the χ^2 fit, so the source slid off to some compromise location as a response to unknown things going on in the zone of obscuration. It was a revelation that we could flip far-field sources between antipodal positions without much influence on the χ^2 fit. However, if the *IRAS* and rich cluster maps are taken at face-value then Perseus-Pisces should largely offset the Great Attractor and the agreement with the microwave background dipole is hard to understand without the Shapley Concentration. On the other hand, if we just make the simple assumption that mass is distributed in a direct way with objects we see, in analogy with the model within 3000 km s^{-1}, then the three distant source model provides a crude description of where galaxies are seen and works wonderfully well with the velocity field. The tentative conclusion is that the Shapley Concentration, projected behind the Great Attractor, provides a comparable additive pull to that of the Great Attractor in contributing to the cosmic microwave background dipole motion in the Local Group rest frame, a possibility first entertained by Scaramella et al. (1989). This region contains about two dozen rich clusters in a sphere of radius 5000 km s^{-1} at a distance of 13,800 km s^{-1} = $157(88/H_0)$ Mpc, and we infer it to have an excess mass of $\sim 1 \times 10^{17}\ M_\odot$. Including consideration of Willick's (1990) observations, coherent flow appears to be generated by the Shapley Concentration across a *radius* of at least 20,000 km s^{-1}.

© American Astronomical Society • Provided by the NASA Astrophysics Data System

1992ApJ...391...16S

4. We offer the very speculative conclusion that M/L values enhanced by a factor in the range 3–10 might be associated with the distant sources. Alternatively, it might be a matter of some other large-scale difference in the characteristics of galaxies or their environments, for example, associated with variations in the ratio of baryonic to dark matter. The hint in this direction comes from the observation that, while there are concentrations of galaxies and clusters just where the velocity field calls for them, there is a question whether the amplitudes are sufficient.

5. At the other extreme on our scale of observations is the "local velocity anomaly." We find that it is a natural consequence of the local distribution of matter inferred from the distribution of galaxies, combined with the tidal squeezing effect of the distant sources. Another apparent influence of the long-range tides is inhibition of a collapse of the nearest groups toward one another. Perturbation velocities in the local anomaly are typically 200 km s^{-1} on a scale of 500 km s^{-1} (see also Han & Mould 1990). This circumstance confirms the jeopardy in local measurements of H_0, particularly that the tendency will be to measure values locally that are too low.

6. Our conclusion that $\Omega_{\rm clumped} \sim 0.03$–$0.1$ is in conflict with the conclusion by Rowen-Robinson et al. (1990) that $\Omega_0 \sim 0.7$ from an equation of the *IRAS* 0.6 Jy survey dipole with the motion inferred from the microwave dipole. We are sensitive to scales smaller than 3000 km s^{-1} while the new *IRAS* redshift survey suggests the dipole motion is developed on scales of 4000–8000 km s^{-1}. However, this difference in scales is probably not enough. Possibly the *IRAS* galaxies are "antibiased" with respect to the peaks in the mass concentration. However, we bet that the real answer is that Rowan-Robinson et al. still do not have a deep enough sample. The motion causing the microwave dipole is probably developed over a substantially larger scale (Scaramella, Vettolani, & Zamorani 1991), so only a fraction is developed within the *IRAS* survey domain, and the value of Ω_0 that Rowan-Robinson et al. should have inferred is only a small fraction of 0.7. We feel that such a high value as $\Omega_0 \sim 0.7$ in clumped matter on scales only a factor 2 above our range of sensitivity can be excluded at a high level of assurance. Unless the clumping that would be implied were contrived to be extremely small on scales smaller than 3000 km s^{-1}, the inevitable result would be local peculiar motions far higher than we observe (see § 5.5). In this respect we concur with the results by Groth, Juszkiewicz, & Ostriker (1989) and those suggested by Ostriker & Suto (1990). Non-Hubble motions are of order 100 km s^{-1} on scales of 1000 km s^{-1} yet, at least in the one situation we can observe, grow to $\sim$600 km s^{-1} on a scale of 15,000 km s^{-1}.

7. Some unfinished business for us is the reconciliation of these results with those by Tully & Shaya (1984) regarding the influence of the Virgo Cluster. Whereas here the Virgo Cluster alone has only a minor influence, the earlier study suggested the cluster has a major effect and we inferred considerably more mass to that concentration, comparable to that implied by virial estimates. An obvious deficiency of the present analysis is the inappropriateness of the linear theory in the proximity of a rich cluster. The earlier work was based on a simplistic spherically symmetric mass model. We cannot claim to have a fully satisfactory model until we understand these rather contradictory results and a nonlinear analysis with a realistic mass distribution is required.

8. Certainly, we can conclude that detailed comparisons of the observed velocity field and light distribution are instructive. Future steps will be to include nonlinear calculations (Peebles 1989, 1990) and to get beyond the insidious assumption of the standard model implicit in the linear equation for peculiar velocities. However, Martel & Wasserman (1990) claim that $\Lambda > 0$ models do not substantially alter peculiar velocities for a fixed Ω_0. Possibly the inverted process of going from velocity field-to-mass distribution being pursued by Bertschinger & Dekel (1990) will ultimately be preferred because it is capable of finding "hidden mass" sources by methods more efficient than our hunt-and-peck efforts. For the moment, our procedure has an advantage because we have a lot more detailed information on the light distribution than we do about the velocity field. We are earnestly trying to diminish that advantage, though, by providing many more galaxy distance estimates. Over the next few years, more detailed velocity field maps should become available, and we should get more precise information on such characteristics as the amplitude in the coherence of galaxy motions as a function of scale and better confirmation of the scale of the mass distribution about luminous galaxies.

We particularly want to thank Roberto Scaramella, Giampaolo Vettolani, and Giovanni Zamorani for making their unpublished map of rich clusters available because this was the final clue. With Jim Peebles, we have been discussing natural extensions for this work involving nonlinear models. Avishai Dekel has kept us informed of progress with the complementary inverse approach of going from velocities to mass distributions. This research has been partially supported by grants from the US National Science Foundation.

REFERENCES

Aaronson, M., et al. 1989, ApJ, 338, 654
Aaronson, M., Bothun, G. D., Mould, J. R., Huchra, J. P., Schommer, R. A., & Cornell, M. E. 1986, ApJ, 302, 536
Aaronson, M., Huchra, J. P., & Mould, J. R. 1979, ApJ, 229, 1
Aaronson, M., Huchra, J. P., Mould, J. R., Schechter, P. L., & Tully, R. B. 1982a, ApJ, 258, 64
Aaronson, M., et al. 1982b, ApJS, 50, 241
Abell, G. O. 1958, ApJS, 3, 211
Abell, G. O., Corwin, H. G., Jr., & Olowin, R. P. 1989, ApJS, 70, 1
Allen, D. A., Norris, R. P., Staveley-Smith, L., Meadows, V. S., & Roche, P. F. 1990, Nature, 343, 45
Bertschinger, E., & Dekel, A. 1989, ApJ, 336, L5
Bertschinger, E., Dekel, A., Faber, S. M., Dressler, A., & Burstein, D. 1990, ApJ, 364, 370
Blumenthal, G. R., Dekel, A., & Primack, J. R. 1988, ApJ, 326, 539
Blumenthal, G. R., Faber, S. M., Primack, J. R., & Rees, M. J. 1984, Nature, 311, 517
Bosma, A., & van der Kruit, P. C. 1979, A&A, 79, 281
Bottinelli, L., Gouguenheim, L., Paturel, G., & Teerikorpi, P. 1986, A&A, 156, 157
Burstein, D., Faber, S. M., & Dressler, A. 1990, ApJ, 354, 18
Byrd, G. G., & Valtonen, M. J. 1985, ApJ, 289, 535
Chincarini, G., & Rood, H. J. 1979, ApJ, 230, 648
Davis, M., & Huchra, J. P. 1982, ApJ, 254, 437
Dekel, A., & Bertschinger, E. 1990, in ASP Conf. Ser., Large-Scale Structures and Peculiar Motions in the Universe, ed. D. W. Latham & L. N. Da Costa (San Francisco: ASP)
de Vaucouleurs, G. 1958, AJ, 63, 253
de Vaucouleurs, G., de Vaucouleurs, A., & Corwin, H. G., Jr. 1976, Second Reference Catalogue of Bright Galaxies (Austin: Univ. of Texas Press)
de Vaucouleurs, G., & Peters, W. L. 1968, Nature, 220, 868
Dressler, A. 1988, ApJ, 329, 519
Dressler, A., Faber, S. M., Burstein, D., Davies, R. L., Lynden-Bell, D., Terlevich, R. J., & Wegner, G. W. 1987, ApJ, 313, L37

© American Astronomical Society • Provided by the NASA Astrophysics Data System

1992ApJ...391...16S

Einasto, J., Kaasik, A., & Saar, E. 1974, preprint
Faber, S. M., & Burstein, D. 1988, in Proc. Vatican Study Week: Large-Scale Motions in the Universe, ed. V. C. Rubin & G. V. Coyne (Princeton Univ. Press), 116
Faber, S. M., & Gallagher, J. S. 1979, ARA&A, 17, 135
Forman, W., Jones, C., & Tucker, W. 1985, ApJ, 293, 102
Geller, M. J., & Huchra, J. P. 1983, ApJS, 52, 61
Giraud, E. 1990, A&A, 231, 1
Groth, E. J., Juszkiewicz, R., & Ostriker, J. P. 1989, ApJ, 346, 558
Han, M., & Mould, J. R. 1990, ApJ, 360, 448
Hoffman, G. L., Olson, D. W., & Salpeter, E. E. 1980, ApJ, 242, 861
Hoffman, G. L., & Salpeter, E. E. 1982, ApJ, 263, 485
Huchra, J. P., & Geller, M. J. 1982, ApJ, 257, 423
Kraan-Korteweg, R. C., Cameron, L. M., & Tammann, G. A. 1986, in Galaxy Distances and Deviations from Universal Expansion, ed. B. F. Madore & R. B. Tully (Dordrecht: Reidel), 65
Lahav, O., Edge, A. C., Fabian, A. C., & Putney, A. 1989, MNRAS, 238, 881
Lilje, P., Yahil, A., & Jones, B. J. T. 1986, ApJ, 307, 91
Lubin, P., & Villela, T. 1986, in Galaxy Distances and Deviations from Universal Expansion, ed. B. F. Madore & R. B. Tully (Dordrecht: Reidel), 169
Lynden-Bell, D., Faber, S. M., Burstein, D., Davies, R. L., Dressler, A., Terlevich, R. J., & Wegner, G. W. 1988, ApJ, 326, 19
Lynden-Bell, D., & Lahav, O. 1988, in Proc. Vatican Study Week: Large-Scale Motions in the Universe, ed. V. C. Rubin & G. V. Coyne (Princeton Univ. Press), 199
Martel, H., & Wasserman, I. 1990, ApJ, 348, 1
McCall, M. L. 1989, AJ, 97, 1341
Meiksin, A., & Davis, M. 1986, AJ, 91, 191
Ostriker, J. P., Peebles, P. J. E., & Yahil, A. 1974, ApJ, 193, L1
Ostriker, J. P., & Suto, Y. 1990, ApJ, 348, 378
Peebles, P. J. E. 1980, in The Large-Scale Structure of the Universe (Princeton University Press)
———. 1989, ApJ, 344, L53
———. 1990, ApJ, 362, 1
Pierce, M. J. 1989, ApJ, 344, L57
———. 1992, in preparation
Pierce, M. J., & Tully, R. B. 1988, ApJ, 330, 579
———. 1991, ApJ, in press
Plionis, M., & Valdarnini, R. 1991, MNRAS, 249, 46
Raychaudhury, S. 1989, Nature, 342, 251
Richter, O. G., Tammann, G. A., & Huchtmeier, W. K. 1987, A&A, 171, 33
Rowan-Robinson, M., et al. 1990, MNRAS, 247, 1
Rubin, V. C. 1951, AJ, 56, 47
———. 1987, in Dark Matter in the Universe, J. Kormendy & G. R. Knapp (Dordrecht: Reidel), 51
Rubin, V. C., Thonnard, N., Ford, W. K., Jr., & Roberts, M. S. 1976, AJ, 81, 719
Sandage, A. 1972, ApJ, 178, 1
Sandage, A., & Tammann, G. A. 1981, Revised Shapley-Ames Catalogue (Washington, DC: Carnegie Institution)
Scaramella, R., Baiesi-Pillastrini, G., Chincarini, G., Vettolani, G., & Zamorani, G. 1989, Nature 338, 562
Scaramella, R., Vettolani, G., & Zamorani, G. 1991, ApJL, in press
Shapley, H. 1930, Harvard Obs. Bull., 874, 9
Shaya, E. J. 1984, ApJ, 280, 470
Shaya, E. J., & Tully, R. B. 1984, ApJ, 281, 56
Smith, S. 1936, ApJ, 83, 23
Staveley-Smith, L., & Davies, R. D. 1989, MNRAS, 241, 787
Strauss, M. A., & Davis, M. 1988, in Proc. Vatican Study Week: Large-Scale Motions in the Universe, ed. V. C. Rubin & G. V. Coyne (Princeton Univ. Press), 256
Tammann, G. A., & Sandage, A. 1985, ApJ, 294, 81
Tonry, J., & Davis, M. 1981, ApJ, 246, 680
Tully, R. B. 1987, ApJ, 321, 280
———. 1988a, Nearby Galaxies Catalog (New York: Cambridge Univ. Press) (NBG Catalog)
———. 1988b, Nature, 334, 209
———. 1988c, AJ, 96, 73
———. 1988d, in Proc. Vatican Study Week: Large-Scale Motions in the Universe, ed. V. C. Rubin & G. V. Coyne (Princeton Univ. Press), 169
———. 1989a, in ASP Colloq.: The Extragalactic Distance Scale, ed. C. J. Pritchet & S. van den Bergh (Provo: Brigham Young Univ. Press), 318
Tully, R. B., & Fisher, J. R. 1977, A&A, 54, 661
———. 1987, Nearby Galaxies Atlas (New York: Cambridge Univ. Press) (NBG atlas)
Tully, R. B., & Fouqué, P. 1985, ApJS, 58, 67
Tully, R. B., & Shaya, E. J. 1984, ApJ, 281, 31
Tully, R. B., Shaya, E. J., & Pierce, M. J. 1992, ApJS, in press (TSP)
White, S. D. M, Frenk, C. S., Davis, M., & Efstathiou, G. 1987, ApJ, 313, 505
Willick, J. 1990, ApJ, 351, L5
Yahil, A. 1985, in The Virgo Cluster of Galaxies, ed. O. G. Richter & B. Binggeli (Garching: ESO), 359
———. 1988, in Vatican Study Week: Large-Scale Motions in the Universe, ed. V. C. Rubin & G. V. Coyne (Princeton Univ. Press), 219
Yahil, A., Sandage, A., & Tammann, G. A. 1977, ApJ, 217, 903
Yahil, A., Walker, D., & Rowan-Robinson, M. 1986, ApJ, 301, L1
Zwicky, F. 1933, Helvetica Phys. Acta., 6, 110

© American Astronomical Society • Provided by the NASA Astrophysics Data System